PERGAMON

International Journal of Multiphase Flow 27 (2001) 1–37

International Journal of Multiphase Flow

www.elsevier.com/locate/ijmulflow

Effect of surfactants on the instability of a liquid thread or annular layer
Part I: Quiescent fluids

S. Kwak, C. Pozrikidis*

Department of Mechanical and Aerospace Engineering, University of California, San Diego, La Jolla, CA 92093-0411, USA

Received 7 October 1999; received in revised form 20 January 2000

Abstract

The effect of an insoluble surfactant on the capillary instability of an annular layer that lines the interior surface of a circular tube and surrounds another annular layer that lines the exterior surface of an inner circular tube is considered. As the radius of the inner cylinder tends to vanish or the radius of the outer cylinder tends to infinity, we obtain either an annular layer coated on the interior or exterior surface of a circular tube, or an infinite thread suspended in a quiescent infinite ambient fluid. In the first part of this paper, a linear stability analysis is carried out for axisymmetric perturbations in the absence or presence of fluid inertia, resulting in a nonlinear algebraic eigenvalue problem whose solution produces the complex phase velocity. When the fluid inertia is negligible, there are two normal modes; one is stable under any conditions, and the second is unstable when the wave length of the perturbation is longer than the circumferential length of the unperturbed interface. Stability graphs are presented to illustrate the properties of the normal modes and their dependence on the ratio of the viscosities of the outer and inner fluid, the surfactant diffusivity, the sensitivity of the surface tension to the surfactant concentration, and the ratio of the cylinder to the thread radius. In all cases, the presence of a surfactant reduces the growth rate of the unstable normal mode but is not able to stabilize the interface. As the surfactant diffusivity is raised, or the surface tension becomes insensitive to the surfactant concentration, the unconditionally stable mode becomes physically irrelevant by requiring an extremely large amplitude of the perturbation in the surfactant concentration, yielding well-known results for uniform surface tension. In the second part of this paper, the nonlinear growth of the instability of an infinite thread is studied under conditions of Stokes flow by dynamical simulation, assuming a linear relationship between the surface tension and the surfactant concentration. The numerical results reveal

* Corresponding author. Tel.: +1-858-534-6530; fax: +1-858-534-7078.
E-mail address: cpozrikidis@ucsd.edu (C. Pozrikidis).

PII: S0301-9322(00)00011-2

that the presence of a surfactant may have a significant effect on the shapes of developing interfacial structures, and that a similarity solution adequately describes the behavior of the thread close to the time of breakup. In the third part of this paper, the instability of an annular layer coated on the interior of a cylindrical tube is considered, with particular reference to bronchial airway collapse. Numerical simulations reveal that the qualitative features of evolution are insensitive to the presence of the surfactant and to the wave length of the perturbation, although both significantly affect the growth rate of the instability. A comparison of the predictions of a thin-layer flow model with the results of the full linear stability theory and with boundary-integral simulations illustrates the capabilities and limitations of the asymptotic approach.

1. Introduction

Capillary instabilities of curved interfaces are encountered in a broad range of natural, engineering, and biophysical applications involving fluid mixing, spraying, atomization, liquid coating and lubrication. Two classes of problems have received special attention: The capillary instability and breakup of a jet or elongated thread suspended in an ambient fluid; and the instability of an annular layer coated on the interior or exterior surface of a cylindrical tube. Recent reviews on these two general topics have been given by Yarin (1993), Grotberg (1994), Papageorgiou (1996), Eggers (1997), Lin and Reitz (1998), Yap and Gaver (1998) and Quéré (1999). Our emphasis in this work is on the effect of an insoluble surfactant.

Laboratory observations have shown that the presence of a surfactant may have an important influence on the instability of a jet or thread and, consequently, on the distribution of the droplet size resulting from breakup (e.g. Burkholder and Berg, 1974). In industrial applications, the process of jet or thread disintegration determines the efficiency of mixing of two stirred immiscible fluids under conditions of laminar or turbulent flow (e.g. Walstra, 1993; Janssen et al., 1994), as well as the effectiveness of industrial equipment in mass transfer chemical engineering processes (Skelland and Walker, 1989; Skelland and Slaymaker, 1990). Milliken et al. (1993) simulated the breakup of an elongated axisymmetric drop in the presence of an insoluble surfactant and in the absence of fluid inertia, and found that variations in surfactant concentration may have a significant influence on the interfacial shapes developing during the nonlinear stages of the motion. A similar influence is expected in the case of an infinite thread, but the precise dependence has not been described by numerical simulation.

A number of authors investigated the effect of a soluble or insoluble surfactant and the significance of interfacial rheology on the linear instability of a liquid jet or thread. Anshus (1973) demonstrated that an insoluble non-diffusing surfactant generally slows down the process of breakup. Burkholder and Berg (1974), Tarr and Berg (1980), Coyle et al. (1981) and Nelson and Berg (1982) studied the effects of surfactant solubility and chemical reaction, and Whitaker (1976) and Hajiloo et al. (1987) accounted for the effects of surface shear and dilatational viscosity; Hansen et al. (1999) allege a sign error in one of Whitaker's equations. In a parallel study, Rabinovich (1979) accounted for the effect of surface diffusivity. More

recently, Elemans et al. (1990) and Pelierne and Lequeux (1991) considered the stability of a thread with varying surface tension due to contamination. Pelierne and Lequeux (1991) tackled the linear stability problem for non-Newtonian fluids and Bousinésq interfaces, but did not explicitly recognize the presence of a surfactant in the governing equations.

Studies of the influence of a surfactant on the stability of an annular layer lining the interior of a tube have been motivated, to a large extent, by applications in pulmonary fluid dynamics. In the lung, a liquid lining protects the cells of the alveolar surface against mechanical damage. The surface tension of the liquid-air interface tends to minimize the interfacial area, and thus favors airway collapse during exhalation. To stabilize the lining, biological surfactants like dipalmitoylphosphatidylcholine, lecithin, and sphingomyelin are naturally secreted from the alveolar type II cells, to reduce the surface tension. The surfactant concentration is a function of the lung volume: It decreases at inspiration due to expansion, and it increases at expiration due to compression to the extent where micelles may develop. Under pathological conditions, such as those responsible for the infant respiratory distress syndrome, IRDS, reduced surfactant concentration may cause alveolar collapse (atelectasis) or the formation of liquid bridges and lenses; both require an increase in effort for breathing (e.g. Hlastala and Berger, 1996). Exogenously delivered surfactants re-open collapsed airways and restore normal breathing.

The effect of a surfactant on airway re-opening and collapse has been studied on several occasions, as reviewed by Grotberg (1994) and Yap and Gaver (1998). It is generally accepted that the physical mechanism responsible for formation of liquid bridges occluding the airways is the Rayleigh capillary instability of a cylindrical interface (Otis et al., 1990, 1993). Airway collapse has been attributed to a combination of the Rayleigh capillary instability and to the relaxation of the tethering forces acting on the external surface of the airways. Otis et al. (1990, 1993) and Halpern and Grotberg (1993) developed a lubrication-flow model that assumes that the wave length of a perturbation is sufficiently larger than the film thickness, and used it to simulate the evolution of the interface subject to axisymmetric perturbations. Their results showed that surfactants decelerate the rate of lens formation due to the increased surfactant concentration at the troughs. To account for the relaxation of the tethering forces, Halpern and Grotberg (1993) studied the instability of a thin annular film coating the interior of a rigid or elastic circular tube using similar methods.

The effect of a surfactant on the instability of an annular layer coated on the exterior of a cylinder tube has also been considered on a few occasions with reference to fiber coating, as reviewed by Quéré (1999). Of particular historical significance is the work by Carroll and Lucassen (1974) who carried out a linear stability analysis for a thin annular layer in the presence of a non-diffusing surfactant, and found that, under extreme conditions, the presence of a surfactant may reduce the growth rate of the most unstable perturbation by a factor of four. Furthermore, Carroll and Lucassen argued that the presence of a surfactant will become increasingly important in the final stages of layer breakup.

In the first part of this paper, we carry out a linear stability analysis of the interface between two concentric annular layers bounded by an inner and an outer cylinder, subject to axisymmetric perturbations. The infinite thread and the annular layer arise as special cases when the radius of the inner or outer cylinder tends to zero or infinity. The present analysis extends previous ones for constant surface tension, including the analysis of

Rayleigh (1878, 1892) who investigated the breakup of an inviscid column or viscous thread suspended in vacuum; the analyses of Weber (1931) and Tomotika (1935) who accounted for a viscous ambient fluid; and the analysis of Goren (1962, 1964) who studied the development of undulations on an annular layer coated on the interior or exterior of a circular tube. Our results will confirm that the presence of a surfactant substantially decreases the growth rate of the instability but is not able to stabilize the interface under any conditions.

In the second part of this paper, we study the nonlinear stages of the instability of an unbounded thread at zero Reynolds number by numerical simulation. The velocity field is computed by a boundary-integral method that employs the periodic Green's function of axisymmetric Stokes flow, and the evolution of the surfactant concentration is computed by a finite-volume method. The results will show that the presence of a surfactant may have an important effect on the shape of interfacial structures developing during the instability and after pinch off, and thus on the number of droplets developing after breakup. Furthermore, the numerical results will allow us to discuss the relevance of a similarity solution developed by Papageorgiou (1995) on the asymptotic behavior of the thread near the time of breakup, in the case of varying surface tension.

In the third part of this paper, we study the instability of an annular layer coated on the interior surface of a cylindrical tube. First, we use the boundary integral method to simulate the evolution of the interface in the particular case where the viscosity of the core fluid is equal to the viscosity of the annular layer, and investigate the effect of a surfactant. Second, we compare the predictions of a flow model based on the thin-layer approximation with those arising by solving the unsimplified equations of Stokes flow. The comparison shows that the viscosity of the core fluid plays an important role when bridges form, and establishes a point of reference for assessing the accuracy of the simplified approach.

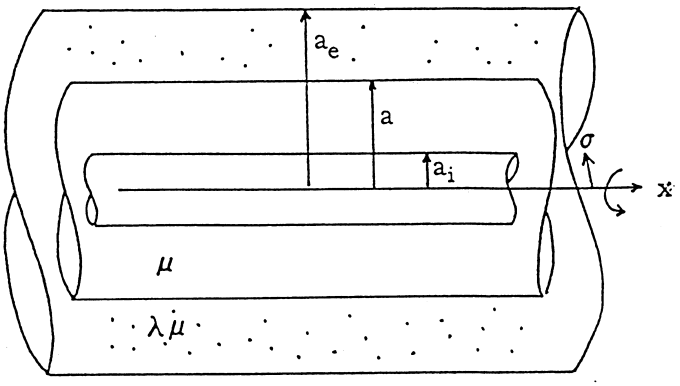

Fig. 1. Illustration of an annular layer coated on the interior surface of an outer concentric circular tube, surrounding another annular layer coated on the exterior surface of an inner concentric circular tube. The interface is populated by an insoluble surfactant.

2. Linear stability analysis for Navier–Stokes flow

Consider the instability of an annular viscous layer coated on the interior surface of an outer circular tube, and surrounding a core fluid that is coated on the exterior surface of an inner circular tube, as illustrated in Fig. 1. As the radius of the inner cylinder tends to vanish and the radius of the outer cylinder tends to infinity, the core fluid reduces to an infinite thread suspended in an infinite quiescent ambient fluid. We assume that the interface is populated by an insoluble surfactant that diffuses along the interface, but not into the bulk of the fluids, and is convected over the interface under the influence of the velocity field caused by the instability. In the unperturbed state, the fluids are quiescent, and the surfactant is distributed uniformly over the interface. We assume further that the effect of gravity is negligible, which amounts to stipulating that an appropriate Bond number is sufficiently large.

We begin by introducing cylindrical polar coordinates (x, σ, φ), with the x axis coinciding with the axis of the thread or annular layer, as shown in Fig. 1. In the unperturbed state, the interface has a cylindrical shape with a circular cross-section of radius a. To carry out a normal-mode analysis subject to axisymmetric perturbations, we describe the radial position of the interface, $f(x, t)$, in terms of the real or imaginary part of the right-hand side of the equation

$$\sigma = f(x, t) = a + \varepsilon a_1 \exp(ik(x\text{-}ct)) \tag{1}$$

where ε is a dimensionless coefficient whose magnitude is much less than unity, a_1 is the complex amplitude of the interfacial perturbation, i is the imaginary unit, k is the wave number, and c is the complex phase velocity.

The motion of the fluid on either side of the interface is governed by the continuity equation and the Navier–Stokes equation with appropriate physical constants corresponding to the properties of the two fluids. Taking advantage of the axial symmetry of the flow, we describe the perturbation flow in terms of the Stokes stream function Ψ_j, where $j = 1$ or 2 for the inner or outer fluid. The axial and radial components of the perturbation velocity are given respectively by

$$u_{x,j} = \varepsilon \frac{1}{\sigma} \frac{\partial \Psi_j}{\partial \sigma}, \quad u_{\sigma,j} = -\varepsilon \frac{1}{\sigma} \frac{\partial \Psi_j}{\partial x} \tag{2}$$

The azimuthal component of the perturbation vorticity is given by

$$\omega = -\varepsilon \frac{1}{\sigma} D^2 \Psi_j \tag{3}$$

where D^2 is a second-order differential operator defined as

$$D^2 = \frac{\partial^2}{\partial x^2} + \frac{\partial^2}{\partial \sigma^2} - \frac{1}{\sigma} \frac{\partial}{\partial \sigma} \tag{4}$$

Substituting these expressions into the azimuthal component of the vorticity transport equation, and linearizing the resulting expression with respect to ε, we derive the fourth-order ordinary differential equation

$$E_j^2 D^2 \Psi_j = 0 \tag{5}$$

where E_j^2 is another second-order differential operator defined as

$$E_j^2 = D^2 - \frac{1}{v_j}\frac{\partial}{\partial t} \tag{6}$$

and v_j is the kinematic viscosity of the jth fluid.

We proceed by expressing the perturbation stream function in the usual normal-mode form

$$\Psi_j = \phi_j(\sigma)\, \exp(ik(x - ct)) \tag{7}$$

Substituting this expression into Eq. (5), we obtain a fourth-order ordinary differential equation for the functions ϕ_j. The general solution was given by Tomotika (1935) in the form

$$\phi_j(\sigma) = \sigma\Big(A_{1,j} I_1(k\sigma) + B_{1,j} K_1(k\sigma) + A_{2,j} I_1\big(k_j\sigma\big) + B_{2,j} K_1\big(k_j\sigma\big)\Big) \tag{8}$$

where $A_{l,j}$ and $B_{l,j}$ are constant coefficients, I_1, K_1 are modified Bessel functions of the first and second kind, and we have introduced the modified complex wave numbers

$$k_j^2 \equiv k^2 - \frac{ick}{v_j} \tag{9}$$

The pressure may be expressed in the corresponding form

$$p_j = \varepsilon X_j(\sigma)\, \exp(ik(x\text{-}ct)) \tag{10}$$

Substituting Eqs. (2), (7), (8) and (10) into the x component of the Navier–Stokes equation, and linearizing with respect to ε, we find

$$X_j(\sigma) = -c\, k\, \rho_j\big(A_{1,j} I_0(k\sigma) - B_{1,j} K_0(k\sigma)\big) \tag{11}$$

Next, we consider the kinematic and dynamic boundary conditions at the interface. Continuity of velocity requires that $\phi_1 = \phi_2$ and $\partial\phi_1/\partial\sigma = \partial\phi_2/\partial\sigma$ at $\sigma = f(x, t)$, where the function $f(x, t)$ determines the location of the interface (Eq. (1)). Applying domain perturbation, we derive the linearized forms

$$\phi_1(a) = \phi_2(a), \qquad \left(\frac{\partial\phi_1}{\partial\sigma}\right)_{\sigma=a} = \left(\frac{\partial\phi_2}{\partial\sigma}\right)_{\sigma=a} \tag{12}$$

The evolution of the deforming interface must be consistent with the motion of fluid particles on either side of the interface. Requiring that the particles do not penetrate the bulk of the fluids, we find

$$\frac{\partial f}{\partial t} + u_x \frac{\partial f}{\partial x} - u_\sigma = 0 \tag{13}$$

where all functions are evaluated at the location of the unperturbed interface. Substituting Eqs. (1), (2), (7) and (8) into Eq. (13), applying once again the method of domain perturbation, and discarding terms that are not constant or which depend linearly on ε, we find the following

expression for the complex amplitude of the perturbation

$$a_1 = \frac{1}{a\,c}\phi_j(\sigma = a) \tag{14}$$

where, in view of Eq. (12), we may set $j = 1$ or 2 on the right-hand side.

To satisfy the kinematic boundary conditions at the surface of cylinders, we require

$$u_{x,1} = \left(\frac{1}{\sigma}\frac{\partial \Psi_1}{\partial \sigma}\right)_{\sigma=a_\mathrm{i}} = 0, \qquad u_{\sigma,1} = -\left(\frac{1}{\sigma}\frac{\partial \Psi_1}{\partial x}\right)_{\sigma=a_\mathrm{i}} = 0 \tag{15}$$

and

$$u_{x,2} = \left(\frac{1}{\sigma}\frac{\partial \Psi_2}{\partial \sigma}\right)_{\sigma=a_\mathrm{e}} = 0, \qquad u_{\sigma,2} = -\left(\frac{1}{\sigma}\frac{\partial \Psi_2}{\partial x}\right)_{\sigma=a_\mathrm{e}} = 0 \tag{16}$$

where a_i, a_e are the radii of the inner or outer cylinder.

The dynamic interfacial condition requires that the jump in the interfacial hydrodynamic traction be balanced by the normal and tangential stresses due to surface tension, so that

$$\left(\boldsymbol{\sigma}^{(1)} - \boldsymbol{\sigma}^{(2)}\right) \cdot \boldsymbol{n} = 2\kappa_m \gamma\, \boldsymbol{n} - \frac{\partial \gamma}{\partial l}\boldsymbol{t} \tag{17}$$

where $\boldsymbol{\sigma}^{(1)}$, $\boldsymbol{\sigma}^{(2)}$ are the stress tensors for the inner or outer fluid, $\boldsymbol{n}$ is the unit vector normal to the interface pointing into the inner fluid, $\kappa_m = 1/2\nabla \cdot \boldsymbol{n}$ is the mean curvature of the interface, and $\boldsymbol{t}$ is the unit vector that is tangential to the interface in an azimuthal plane and points in the direction of increasing arc length l. All functions in (17) are evaluated at the location of the unperturbed interface. Using Eq. (1) and standard expressions for the normal vector and mean curvature (e.g. Pozrikidis, 1997), we derive the linearized form

$$\boldsymbol{n} = -\boldsymbol{e}_\sigma + \varepsilon i k a_1 \exp(ik(x - ct))\boldsymbol{e}_x \tag{18}$$

where $\boldsymbol{e}_x$ and $\boldsymbol{e}_\sigma$ are the unit vectors in the axial and radial directions, and

$$2\kappa_m = -\frac{1}{a} + \varepsilon\frac{a_1}{a^2}(1 - k^2a^2)\exp(ik(x - ct)) \tag{19}$$

Subject to a normal-mode perturbation, the surface tension assumes the usual functional form

$$\gamma = \gamma_0 + \varepsilon\gamma_1 \exp(ik(x - ct)) \tag{20}$$

where γ_0 is the surface tension in the unperturbed state, and γ_1, is a complex constant to be determined as part of the solution.

Substituting Eqs. (18)–(20) into Eq. (17), and linearizing both sides with respect to ε, we obtain the following two scalar boundary conditions for the tangential and normal components:

$$\mu_1\left(\frac{\partial u_{x,1}}{\partial \sigma}+\frac{\partial u_{\sigma,1}}{\partial x}\right)-\mu_2\left(\frac{\partial u_{x,2}}{\partial \sigma}+\frac{\partial u_{\sigma,2}}{\partial x}\right)=\varepsilon ik\gamma_1\exp(ik(x-ct)) \tag{21}$$

and

$$-p_1+2\mu_1\frac{\partial u_{\sigma,1}}{\partial \sigma}+p_2-2\mu_2\frac{\partial u_{\sigma,2}}{\partial \sigma}=\frac{\varepsilon}{a^2}\left(-a_1(1-k^2a^2)\gamma_0+a\gamma_1\right)\exp(ik(x-ct)) \tag{22}$$

where both sides are evaluated at the location of the unperturbed interface, at $\sigma = a$.

The surface tension, γ, is a function of local surfactant concentration, Γ. The evolution of the latter is governed by the convection-diffusion equation

$$\frac{\mathrm{d}\Gamma}{dt}=-\boldsymbol{u}\cdot\boldsymbol{t}\frac{\partial \Gamma}{\partial l}-\frac{\Gamma}{\sigma}\frac{\partial(\sigma\boldsymbol{u}\cdot\boldsymbol{t})}{\partial l}-\Gamma 2\kappa_m\boldsymbol{u}\cdot\boldsymbol{n}+\frac{D_\mathrm{s}}{\sigma}\frac{\partial}{\partial l}\left(\sigma\frac{\partial \Gamma}{\partial l}\right) \tag{23}$$

where D_s is the surfactant diffusivity, and the derivative $\mathrm{d}/\mathrm{d}t$ on the left-hand side expresses the rate of change of a variable following the motion of interfacial marker points moving with the component of the velocity of the fluid normal to the interface. Eq. (23) states that changes in the surfactant concentration are due to convection and diffusion, as well as to condensation or dilution due to interfacial compression or expansion. Linearizing Eq. (23) with respect to ε, we obtain

$$\frac{\partial \Gamma}{\partial t}=-u_x\frac{\partial \Gamma}{\partial x}-\Gamma\frac{\partial u_x}{\partial x}-\Gamma 2\kappa_m u_\sigma+D_s\frac{\partial^2\Gamma}{\partial x^2} \tag{24}$$

where both sides are evaluated at $\sigma = a$. Anticipating now that the functional form of the surfactant concentration is consistent with that of a normal-mode perturbation, we write

$$\Gamma=\Gamma_0+\varepsilon\Gamma_1\exp(ik(x-ct)) \tag{25}$$

where Γ_0 is the surfactant concentration at the unperturbed state, which is assumed to be constant, and Γ_1 is the complex amplitude of the surfactant concentration to be determined as part of the solution. Substituting expressions (2), (19), (8), and (25) into Eq. (24), and linearizing the resulting equation with respect to ε, we determine that the complex constant Γ_1 has the following form

$$\begin{aligned}\frac{\Gamma_1}{\Gamma_0}=\frac{ik}{\left(-ikc+k^2D_s\right)a}\Big\{&A_{1,j}\left[kaI_0(ka)-I_1(ka)\right]+A_{2,j}\left[k_jaI_0\left(k_ja\right)-I_1\left(k_ja\right)\right]\\&-B_{1,j}\left[kaK_0(ka)+K_1(ka)\right]-B_{2,j}\left[k_jaK_0\left(k_ja\right)+K_1\left(k_ja\right)\right]\Big\}\end{aligned} \tag{26}$$

When the concentration of the surfactant lies below the saturation level, a linear relationship may be assumed between the surface tension and the surfactant concentration (Adamson, 1982). Gibbs' theory gives

$$\gamma_\mathrm{c}-\gamma=\Gamma RT \tag{27}$$

where R is the ideal gas constant, T is the absolute temperature, and γ_c is surface tension of a

clean interface that is devoid of surfactants. It is a common practice to express the sensitivity of the surface tension to the surfactant concentration in the terms of the dimensionless physicochemical parameter

$$\beta = \frac{\Gamma_0 RT}{\gamma_c} \tag{28}$$

Eq. (27) then assumes the equivalent form:

$$\gamma = \frac{\gamma_0}{1-\beta}\left(1 - \frac{\Gamma}{\Gamma_0}\beta\right) \tag{29}$$

Setting $\Gamma = 0$ yields the following relation between the unperturbed-state surface tension and that of a clean interface

$$\gamma_0 = (1-\beta)\ \gamma_c \tag{30}$$

In the context of linear stability theory, a linear relation between γ and Γ may be derived by expanding the generally nonlinear function $\gamma(\Gamma)$ in a Taylor series about the unperturbed concentration, and then truncating the expansion after the linear term. The coefficient of the linear term, known as the interface elasticity, however, is no longer related to R and T as shown in Eq. (27). To avoid making this distinction, we shall continue to use the relation (27), bearing in mind its generalization.

Substituting Eqs. (20) and (25) into Eq. (29), we derive the following expression for the complex amplitude of the surface tension

$$\frac{\gamma_1}{\gamma_0} = -\beta\frac{\Gamma_1}{\Gamma_0} \tag{31}$$

where the ratio Γ_1/Γ_0 is given in Eq. (26). Note that when $\beta = 0$, in which case the surface tension is insensitive to the surfactant concentration, the right-hand side of (31) reduces to zero. Due to the limitations of the linear model, the range of values of the sensitivity parameter β considered, would be less than 0.5; higher values may result in negative surface tension.

Collecting the kinematic and dynamic boundary conditions expressed by Eqs. (12), (15), (16), (21) and (22), and using the derived expressions for the velocity, pressure, surface tension, and mean curvature, we formulate a homogeneous system of eight equations for the eight unknown coefficients $A_{i,j}$ and $B_{i,j}$ where $i, j = 1, 2$, of the form

$$\boldsymbol{M}\boldsymbol{w} = \boldsymbol{0} \tag{32}$$

where $\boldsymbol{0}$ is a null vector, $\boldsymbol{w}$ is a vector of unknown coefficients defined as

$$\boldsymbol{w}^{\mathrm{T}} = \left[A_{1,1}, A_{2,1}, B_{1,1}, B_{2,1}, A_{1,2}, A_{2,2}, B_{1,2}, B_{2,2}\right] \tag{33}$$

and

$$\boldsymbol{M} = \begin{bmatrix} I_1(ka) & I_1(k_1a) & K_1(ka) & K_1(k_1a) & -I_1(ka) & -I_1(k_2a) & -K_1(ka) & -K_1(k_2a) \\ kI_0(ka) & k_1I_0(k_1a) & -kK_0(ka) & -k_1K_0(k_1a) & -kI_0(ka) & k_2I_0(k_2a) & kK_0(ka) & k_2K_0(k_2a) \\ I_1(ka_i) & I_1(k_1a_i) & K_1(ka_i) & K_1(k_1a_i) & 0 & 0 & 0 & 0 \\ kI_0(ka_i) & k_1I_0(k_1a_i) & -kK_0(ka_i) & -k_1K_0(k_1a_i) & 0 & 0 & 0 & 0 \\ 0 & 0 & 0 & 0 & I_1(ka_e) & I_1(k_2a_e) & K_1(ka_e) & K_1(k_2a_e) \\ 0 & 0 & 0 & 0 & kI_0(ka_e) & k_2I_0(k_2a_e) & -kK_0(ka_e) & -k_2K_0(k_2a_e) \\ F_1 & F_2 & F_3 & F_4 & F_5 & F_6 & F_7 & F_8 \\ G_1 & G_2 & G_3 & G_4 & G_5 & G_6 & G_7 & G_8 \end{bmatrix}$$

Lengthy expressions for the functions F_i and G_i in terms of Bessel functions are given in Appendix A. Setting the determinant of the matrix $\boldsymbol{M}$ equal to zero, we obtain a non-polynomial algebraic equation for the complex phase velocity c. The number of solutions corresponding to distinct normal modes could not be assessed except in the limit of Stokes flow, as will be discussed in Section 3.

When the inner cylinder is absent, we obtain an annular layer surrounding a liquid thread. For the velocity to be regular at the axis, the constants $B_{1,1}$ and $B_{2,1}$ must be set equal to zero, yielding the following simplified expressions for the interior stream function:

$$\Psi_1 = \sigma\big(A_{1,1}I_1(k\sigma) + A_{2,1}I_1(k_1\sigma)\big)\exp(ik(x-ct)) \tag{35}$$

The linear system (34) undergoes analogous simplifications.

In the second special case, we consider an annular layer coated on the exterior surface of a cylindrical tube while surrounded by an infinite outer fluid. To ensure regular behavior at infinity, we set the coefficients $A_{1,2}$ and $A_{2,2}$ equal to zero, and obtain the following simplified form for the exterior stream function:

$$\Psi_2 = \sigma\big(B_{1,2}K_1(k\sigma) + B_{2,2}K_1(k_2\sigma)\big)\exp(ik(x-ct)) \tag{36}$$

The linear system (34) undergoes analogous simplifications.

In the simplest configuration, both the internal and external cylinders are absent, and we obtain a thread suspended in an infinite ambient fluid. The stream functions for the internal and external flow are described, respectively, by Eqs. (35) and (36), and the linear system (34) undergoes analogous simplifications. In the absence of a surfactant, the matrix in (34) reduces to that presented by Tomotika (1935) for constant surface tension.

3. Linear stability analysis for Stokes flow

When inertia is negligible within both fluids, the modified complex wave numbers k_j reduce to the real wave number k, and Eq. (8) no longer provides us with the general solution. To study this limit, we expand the modified wave numbers k_1 and k_2 and the Bessel functions in the last two terms on the right-hand side of (8) in Taylor series with respect to the

dimensionless phase velocities $\hat{c}_j = ic/(kv_j)$ about k for $j = 1, 2$. Demanding that the resulting expression satisfies the equations of Stokes flow to first-order with respect to $\hat{c}_j$, we derive Tomotika's (1935) expression

$$\Psi_j(\sigma) = \sigma\Big(C_{1,j} I_1(k\sigma) + D_{1,j} K_1(k\sigma) + C_{2,j} \frac{1}{2}\sigma\big(I_0(k\sigma) + I_2(k\sigma)\big) - D_{2,j} \frac{1}{2}\sigma\big(K_0(k\sigma) + K_2(k\sigma)\big)\Big) \exp(ik(x - ct)) \tag{37}$$

where $C_{l,j}$ and $D_{l,j}$ are new coefficients. Working as previously, we obtain the linear system (32), where the vector of unknowns is defined as

$$\boldsymbol{w}^{\mathrm{T}} = \big[C_{1,1}, C_{2,1}, D_{1,1}, D_{2,1}, C_{1,2}, C_{2,2}, D_{1,2}, D_{2,2}\big] \tag{38}$$

and the coefficient matrix is given by

$$\boldsymbol{M} = \begin{vmatrix} I_1(ka) & H_1 & k_1(ka) & H_2 & -I_1(ka) & H_3 & -K_1(ka) & H_4 \\ kI_0(ka) & L_1 & -kK_0(ka) & L_2 & -kI_o(ka) & L_3 & kK_o(ka) & L_4 \\ I_1(Ka_i) & N_1 & K_1(ka_i) & N_2 & 0 & 0 & 0 & 0 \\ kI_0(ka_i) & N_3 & -kK_0(ka_i) & N_4 & 0 & 0 & 0 & 0 \\ 0 & 0 & 0 & 0 & I_i(ka_{\mathrm{e}}) & Q_1 & K_1(ka_{\mathrm{e}}) & Q_2 \\ 0 & 0 & 0 & 0 & kI_0(ka_{\mathrm{e}}) & Q_3 & -kK_0(ka_{\mathrm{e}}) & Q_4 \\ S_1 & S_2 & S_3 & S_4 & S_5 & S_6 & S_7 & S_8 \\ T_1 & T_2 & T_3 & T_4 & T_5 & T_6 & T_7 & T_8 \end{vmatrix} \tag{39}$$

Expressions for the entries H_i, L_i, N_i, Q_i, S_i, and T_i are given in Appendix B. In the case of an internally bounded annular layer, an externally bounded annular layer, or an unbounded thread, the linear system (34) and the matrix (39) undergo straightforward simplifications, as discussed in the preceding section.

Alternatively, we may solve the following set of equations in place of (5)

$$D^2\Psi_j = \Psi_j^*, \qquad D^2\Psi_j^* = 0 \tag{40}$$

and work with the general solution

$$\Psi_j(\sigma) = \sigma\big(E_{1,j} I_1(k\sigma) + F_{1,j} K_1(k\sigma) + E_{2,j}\sigma I_0(k\sigma) + F_{2,j}\sigma K_0(k\sigma)\big) \exp(ik(x\text{-}ct)) \tag{41}$$

derived by Goren (1962), where $E_{l,j}$ and $F_{l,j}$ are the new coefficients. The properties of the Bessel functions ensure that expression (41) reduces to (37) by an appropriate grouping of the coefficients. With the choice (41), we obtain the linear system (32), where the vector of unknowns is defined as

$$\boldsymbol{w}^{\mathrm{T}} = \big[E_{1,1}, E_{2,1}, F_{1,1}, F_{2,1}, E_{1,2}, E_{2,2}, F_{1,2}, F_{2,2}\big] \tag{42}$$

and the coefficient matrix is given by

$$\boldsymbol{M} = \begin{vmatrix} I_1(ka) & aI_0(ka) & K_1(ka) & aK_0(ka) & -I_1(ka) & -aI_0(ka) & -K_1(ka) & -aK_0(ka) \\ kI_0(ka) & \hat{L}_1 & -kK_0(ka) & \hat{L}_2 & -kl_0(ka) & \hat{L}_3 & kK_0(ka) & \hat{L}_4 \\ l_1(ka_{\rm i}) & a_{\rm i}I_0(ka_{\rm i}) & K_1(ka_{\rm i}) & a_{\rm i}K_0(ka_{\rm i}) & 0 & 0 & 0 & 0 \\ kI_0(ka_{\rm i}) & \hat{N}_3 & -kK_0(ka_{\rm i}) & \hat{N}_4 & 0 & 0 & 0 & 0 \\ 0 & 0 & 0 & 0 & I_1(ka_{\rm e}) & a_{\rm e}I_0(ka_{\rm e}) & K_1(ka_{\rm e}) & a_{\rm e}K_0(ka_{\rm e}) \\ 0 & 0 & 0 & 0 & kI_0(ka_{\rm e}) & \hat{Q}_3 & -kK_0(ka_{\rm e}) & \hat{Q}_4 \\ S_1 & \hat{S}_2 & S_3 & \hat{S}_4 & S_5 & \hat{S}_6 & S_7 & \hat{S}_8 \\ T_1 & \hat{T}_2 & T_3 & \hat{T}_4 & T_5 & \hat{T}_6 & T_7 & \hat{T}_8 \end{vmatrix} \tag{43}$$

Expressions for the entries $\hat{L}_i$, $\hat{N}_i$, $\hat{Q}_i$, $\hat{S}_i$, and $\hat{T}_i$ are given in Appendix B. The second and sixth columns of (43) arise, respectively, by dividing the first or fifth column of (39) by k, and adding the result to the second or sixth column, as shown in Appendix B. The fourth and eighth column of (39) arise, respectively, by dividing the third or seventh column of (39) by k, adding the result to the fourth or eighth column, and then switching the sign of the resulting expressions, as shown in Appendix B.

Eliminating the denominators from all elements of matrix (39) or (43), by multiplying corresponding rows by them, setting the determinant of the resulting matrix equal to zero, and simplifying the resulting expressions, we obtain a cubic equation for the complex phase velocity c. This equation has a double real root and a single real root, revealing the existence of two normal modes. One of these modes is always stable, while the second is unstable when the reduced wave number ka is less than 1.0, and stable when the reduced wave number ka is larger than 1.0. In all cases, the sinusoidal perturbation in the surfactant concentration is either in phase, or has a 180° phase shift with respect to that of the radial interfacial displacement, as required by the absence of a mean flow. When the surface tension is constant, that is, in the absence of a surfactant, the cubic equation for c reduces to a linear equation yielding a single normal mode, in agreement with the results of previous analyses.

The occurrence of two normal modes in the presence of surfactant can be explained by the following arguments. An arbitrary monochromatic perturbation disturbs the surfactant concentration and radial position of the interface with a wave of arbitrary amplitude and arbitrary phase shift. A normal mode perturbation requires a specific ratio between the properly reduced amplitudes in concentration and deformation, and a specific value for the phase shift. Counting the number of unknowns involved in the decomposition of the arbitrary concentration and deformation waves into normal modes, reveals that only two modes are necessary. When the surface tension is constant, the perturbation in concentration is dynamically irrelevant, and the stable normal mode disappears, as will be described later in this section. It may be argued that similar arguments can be made for the more general case of Navier–Stokes flow, but the generalization is not appropriate: only in Stokes flow specifying the instantaneous interfacial geometry, distribution of boundary velocity and interfacial traction uniquely determines the flow.

Deriving the explicit form of the generally cubic secular equation whose solution provides us with the complex phase velocity, requires a large amount of algebra and was not attempted. As a practical alternative, we compute the four real coefficients of the cubic polynomial using five-

point finite differences, where the determinant of the regularized matrix is evaluated from the LU decomposition. The real roots of the cubic polynomial are then found analytically using Cardano's formula.

3.1. Case studies

We proceed now to present and discuss interface stability for several cases, illustrating the effect of five dimensionless parameters including the radii ratios a_i/a and a_e/a, the physicochemical constant β defined in Eq. (28), the viscosity ratio $\lambda = \mu_2/\mu_1$, and the surfactant diffusivity expressed by the property number

$$\alpha = \frac{a\gamma_0}{\mu D_s} \tag{44}$$

As α tends to zero, the surfactant diffuses more readily over the interface, and the motion occurs under uniform but time-dependent surface tension.

To begin, we consider the instability of a thread suspended in vacuum. In Fig. 2(a), we plot the dimensionless growth rate $\hat{\Sigma}_I = \mu k c_I a/\gamma_0$ for the conditionally unstable normal mode against the reduced wave number ka for several values of β, for the case $\alpha = 1.0$ and $\lambda = 0$; c_I is the imaginary part of the complex phase velocity. The line marked $\beta = 0$ corresponds to constant surface tension, $\gamma = \gamma_0$. In this case, as ka becomes smaller, the growth rate increases in a monotonic fashion and tends to a nonzero value. In contrast, in the presence of an active surfactant, $\beta \neq 0$, as ka is reduced from the value of unity, the growth rate reaches a maximum at a nonzero value of ka and then tends to a small but nonzero value. We note that, under constant surface tension, maximum growth rate occurs at a nonzero wave number for nonzero and non-infinite value of λ (Tomotika, 1935), and this suggests that the surfactant acts to increase the viscosity of the ambient fluid. A second important feature evident from Fig. 2(a) is that the presence of a surfactant substantially reduces the growth rate of the conditionally unstable mode, especially for moderate and small wave numbers, but it is not able to stabilize the interface. As ka tends to zero, the growth rate of the stable normal mode tends to a negative value that is independent of the parameter β. As ka is raised from zero to higher values, the magnitude of the negative growth rate increases rapidly at a seemingly exponential rate, yielding a fast decay.

The results of the linear stability analysis show that the sinusoidal perturbation in the surfactant concentration is in phase with that of the interfacial deformation. In Fig. 2(b), we plot the ratio of the reduced amplitude of the concentration and interfacial perturbation, $\delta \equiv (\Gamma_1/\Gamma_0)/(a_1/a)$, for the unstable mode discussed in Fig. 2(a). As ka is raised, the magnitude of δ decreases monotonically from the value of unity to zero, and vanishes when ka has reached the stability threshold. In contrast, as ka is raised, the magnitude of δ for the stable mode increases at an accelerating rate. Physically, the stable mode requires an increasingly larger perturbation in the surfactant concentration with respect to the unperturbed value. Because of this behaviour, in practice, an arbitrary perturbation is expected to consist mainly of the unstable normal mode. As the sensitivity of the surface tension to the surfactant concentration β is diminished, the unstable normal mode reduces to that for a thread with a clean interface, as shown in Fig. 2(b), whereas the stable normal mode disappears by requiring

a virtually infinite perturbation in the surfactant concentration in order to survive (Kwak, 1999).

Results similar to those presented in Fig. 2 were obtained for nonzero values of the viscosity ratio (Kwak, 1999). Parametric studies revealed a diminishing sensitivity of the growth rate on β with increasing λ due to the increasing significance of the motion of the outer fluid on the interfacial force balance. For example, when $\lambda = 1$, $\hat{\Sigma}_I$ decreases only by a few percent as β is raised from 0 to 0.5. In contrast, the amplitude ratio δ for the stable normal mode remains a sensitive function of β for the reasons stated in the previous paragraphs.

Next, we investigate the effect of the property number α expressing the surfactant diffusivity. In Fig. 3, we present a graph of the reduced growth rate for the unstable normal mode, plotted against α on a log-linear scale, for $\lambda = 0$, 1, $\beta = 0.5$, and $ka = 0.5$. When α is small, surfactant diffusion dominates convection, the surfactant concentration is nearly uniform, and the motion is similar to that occurring under constant surface tension. As α is raised, convection generates significant surfactant concentration gradients that cause the development of inhomogeneities in surface tension. Finally, surfactant diffusion becomes insignificant when α is larger than 100. Fig. 3 shows that the growth rate of the unstable mode is sensitive to the surfactant diffusivity for $\lambda = 0$ but not for $\lambda = 1$, for reasons discussed in the previous paragraph. In contrast, the

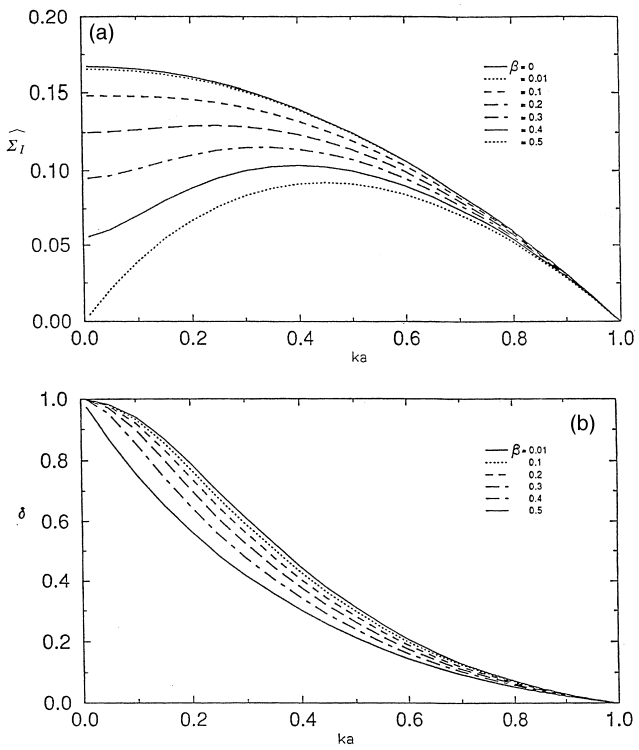

Fig. 2. Instability of a thread suspended in an inviscid ambient fluid, $\lambda = 0$, for $\alpha = 1.0$, and $\beta = 0.5$, 0.4, 0.3, 0.2, 0.1, 0.01. (a) Graphs of the dimensionless growth rate and (b) ratio of the reduced amplitude of the concentration and interfacial waves, $\delta \equiv (\Gamma_1/\Gamma_0)/(a_1/a)$ for the unstable normal mode.

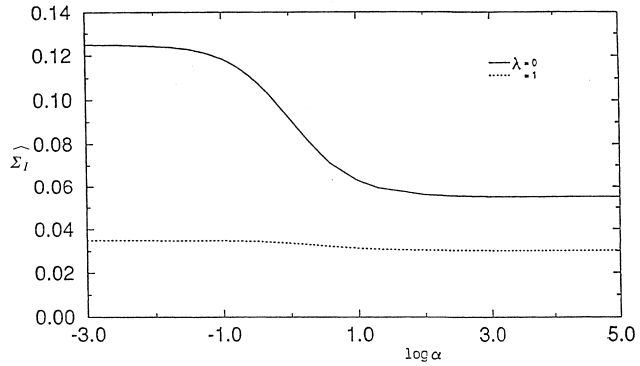

Fig. 3. Instability of a thread suspended in an inviscid or viscous ambient fluid, $\lambda = 0$, 1, for $\beta = 0.5$, subject to a perturbation with $ka = 0.5$. The graphs illustrate the effect of the surfactant diffusivity, expressed by the parameter α, on the growth rate of the unstable normal mode.

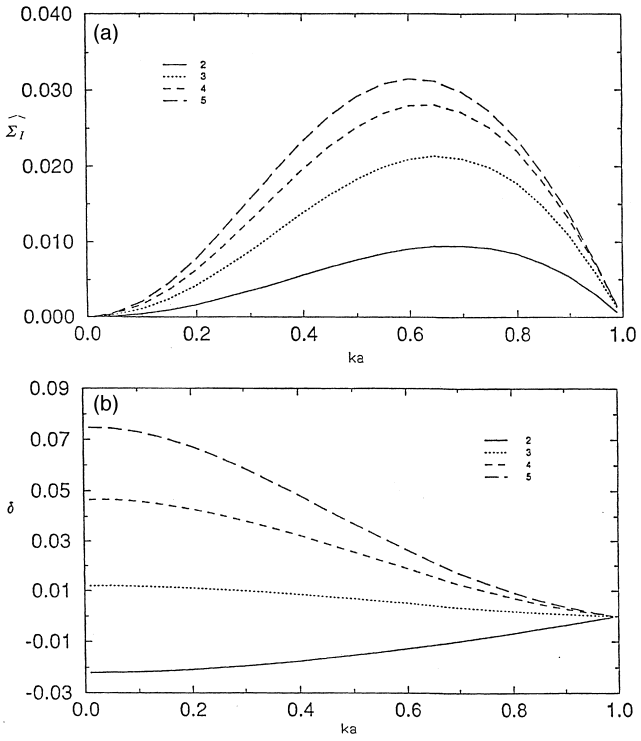

Fig. 4. Instability of a core-annular arrangement for $\lambda = 1$, $\beta = 0.5$, $\alpha = 1$, $a_e/a = 2$, 3, 4, 5. (*a*) Reduced growth rate and (b) ratio of the reduced amplitudes of the concentration and height of the interfacial waves for the unstable normal mode.

growth rate of the stable mode is determined to be sensitive to the surfactant diffusivity irrespective of the viscosity ratio.

We proceed now to discuss the influence of the internal and external cylinders on the properties of the normal modes. In Fig. 4(a), we present graphs of the reduced growth rates of the unstable normal modes for a core-annular arrangement — in the absence of the inner cylinder but in the presence of an outer cylinder — for $\lambda = 1$, $\beta = 0.5$, $\alpha = 1$, and $a_e/a = 2$, 3, 4, 5. Fig. 4(a) reveals a significant reduction in the growth rate of the unstable mode as the outer cylinder approaches the interface, accompanied by a noticeable shifting of the wave number for maximum growth towards higher values. This behavior contrasts with the insensitivity of the growth rate of the stable mode. The behavior of the ratio of the concentration and interface amplitudes δ for the unstable normal mode is illustrated in Fig. 4(b). An interesting new feature, in comparison with the unbounded thread, is that, as the cylinder radius a_e is reduced from $3a$ to $2a$, δ takes negative values for both modes and for all wave numbers, indicating that a maximum in the interface deformation corresponds to a minimum in the surfactant concentration distribution. A physical explanation for this inversion could not be found.

In Fig. 5(a) and (b), we present results for an annular film coated on the exterior surface of a tube in the presence of an inner cylinder but in the absence of an outer cylinder — for $\lambda = 1$,

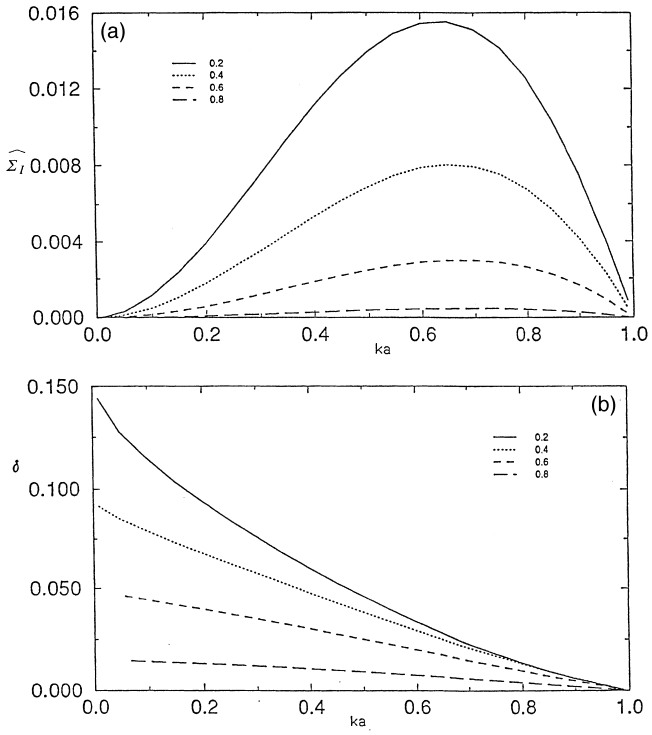

Fig. 5. Instability of an annular layer coated on the exterior surface of a tube for $\lambda = 1$, $\beta = 0.5$, $\alpha = 1$, and $a_i/a = 0.2$, 0.4, 0.6, 0.8. (a) Reduced growth rate and (b) ratio of the reduced amplitudes of the concentration and height of the interfacial waves for the unstable normal mode.

$\beta = 0.5$, $\alpha = 1$, and for $a_i/a = 0.2$, 0.4, 0.6, 0.8. The behavior of the growth rate and of the reduced amplitude ratio is qualitatively similar to those described in the previous paragraph. As the inner cylinder approaches the interface, δ remains positive for all wave numbers, which contrasts with the inversion sign observed for the core-annular arrangement. These differences attest to the subtlety of the capillary instability in the presence of a surfactant. Additional results for unstable and stable normal modes, and for externally and internally bounded arrangements are presented by Kwak (1999).

4. Nonlinear instability of an infinite thread

In the second part of this paper, we study the nonlinear instability of the infinite thread under conditions of Stokes flow, by numerical simulation. The numerical method involves two main components: Computation of the instantaneous interface velocity using a boundary-integral method; and updating of the surfactant concentration using a finite-volume method. The governing equations and numerical implementation are discussed by Pozrikidis (1998, 1999). Briefly, to describe the motion of the interface, we trace one period of it in a meridional plane with a set of marker points, typically on the order of 100; we approximate the contour of the interface with a collection of circular arcs; we solve the integral equation for the velocity at the position of the point particles using a boundary-element method; and we advance the position of the point particles and the surfactant concentration using the first- or second-order Runge–Kutta method. Points are added at regions of large curvature, or when two adjacent marker points have been separated by a large distance due to stretching. The surfactant concentration at the new points is computed by quadratic interpolation. Numerical error causes the volume of the thread over a period to decrease slightly during the simulations, but the change was less than 0.5% in all cases, and less that 0.1% in most cases. The change in the total amount of the surfactant over one period was less than 0.1% in all cases. Each simulation requires approximately 48 h of CPU time on a SUN SPARCstation 20.

In the majority of the simulations, the radial position of the interface and the concentration of the surfactant are set in a manner that is consistent with the properties of the normal modes, subject to conservation of thread volume and total amount of the surfactant over each period. Specifically, the initial shape of the interface and surfactant concentration are given by

$$\sigma = a_{-1} + a_1 \cos(kx), \quad \Gamma = \Gamma_{-1} + \Gamma_1 \cos(kx) \tag{45}$$

where the coefficient a_1 is given an arbitrary value, and the coefficients a_{-1}, Γ_{-1}, Γ_1 are computed so as to satisfy the aforementioned constraints.

First, we confirm that the numerical results are consistent with predictions of linear stability theory in the limit of small-amplitude perturbations. In Fig. 6, we plot the ratio A/a_1 against the reduced time $\hat{t} = \gamma t/(\mu a)$ for an interface perturbed by an unstable normal mode, for $\beta = 0.5$, $\alpha = 1$, $\lambda = 0$, 1, and for a perturbation with $ka = 0.5$ and initial amplitude $a_1/a = 0.01$; A is half the difference between the maximum and minimum interface radial position. The results reveal an exponential initial growth at a rate that is virtually identical to that predicted by linear theory. Nonlinear interactions and inevitable numerical contamination cause deviation from the exponential growth at long times.

Fig. 7(a) and (b) shows characteristic stages in the evolution of a thread with $\lambda = 1$, $\beta = 0.5$, $\alpha = 1, 100$, subject to an unstable normal-mode perturbation with reduced wave length $ka = 0.5$ and a moderate amplitude $a_1/a = 0.2$. For $\alpha = 1$, reference to Fig. 2(a) shows that this wave number is close to that for maximum growth rate; for $\alpha = 100$, maximum growth rate occurs approximately at $ka = 0.575$. The evolving profiles shown in Fig. 7(a) and (b) clearly illustrate that the presence of the surfactant may have a significant influence not only on the growth rate of the instability, but also on the shapes of the developing interfacial patterns. When $\alpha = 1$, the surfactant diffuses readily over the interface, the distribution of the surfactant concentration shows only mild variations, as illustrated in Fig. 7(c), and the motion is similar to that occurring under constant surface tension discussed by Newhouse and Pozrikidis (1992), Lister and Stone (1998) and Pozrikidis (1999). At long times, the thread breaks up into a sequence of drops connected by spindle-like links. When $\alpha = 100$, on the other hand, the onset of large concentration gradients due to convection, as illustrated in Fig. 7(d), generate Marangoni tractions that cause the spindle-like links to develop bulged shapes. In this case, the concentration distribution develops four maxima and two minima over each period. Three satellite drops are expected to develop within each period after the thread has broken up at the points of minimum cross-section.

Further simulations showed that the wave length of the disturbance has a strong influence on the behavior of the thread at long times. As the reduced wave number ka is raised towards the critical value of unity, the primary drops become larger, and the connecting links obtain spindle-like shapes similar to those shown in Fig. 7(a). On the other hand, as the reduced wave number becomes smaller, subharmonic waves amplify within each period, causing the formation of multiple drops connected by multiple spindles. The number, size, and shapes of the drops and links depend on the surfactant distribution established at long times. In addition, the numerical results revealed that the subharmonic waves influence the critical time of thread breakup, $\hat{t}_c$, in a subtle fashion; a simple relationship between the initial disturbance wave number and $\hat{t}_c$ is not apparent. These features are illustrated in Fig. 8(a) and (b) for a thread with $\lambda = 1$, $\beta = 0.5$, $\alpha = 100$, and $ka = 0.9, 0.2$; the evolution for $ka = 0.5$ was displayed in Fig. 7(b). A tabulation of the number of the developing satellite drops in terms of β and α

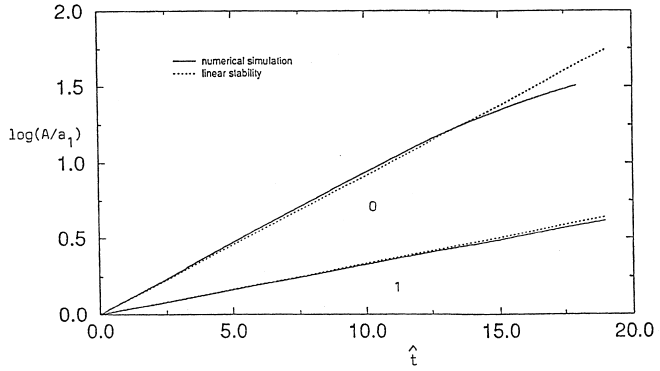

Fig. 6. Numerical simulation of the instability of a thread suspended in an infinite ambient fluid for $\lambda = 0$, 1, $\beta = 0.5$, $\alpha = 1$, and $ka = 0.5$. Graph of the reduced amplitude of the perturbation showing agreement with linear stability analysis for the unstable normal mode.

would be useful as an engineering resource, but requires a large amount of work and was not attempted.

Similar behavior was observed for threads with viscosity ratios larger than unity. In all cases, when the parameter α is sufficiently high, the spindle-like links connecting the primary drops develop secondary instabilities that give rise to wobbly profiles. When λ is set to a very large value, yielding an inviscid thread suspended in a viscous ambient fluid, and the wave number is

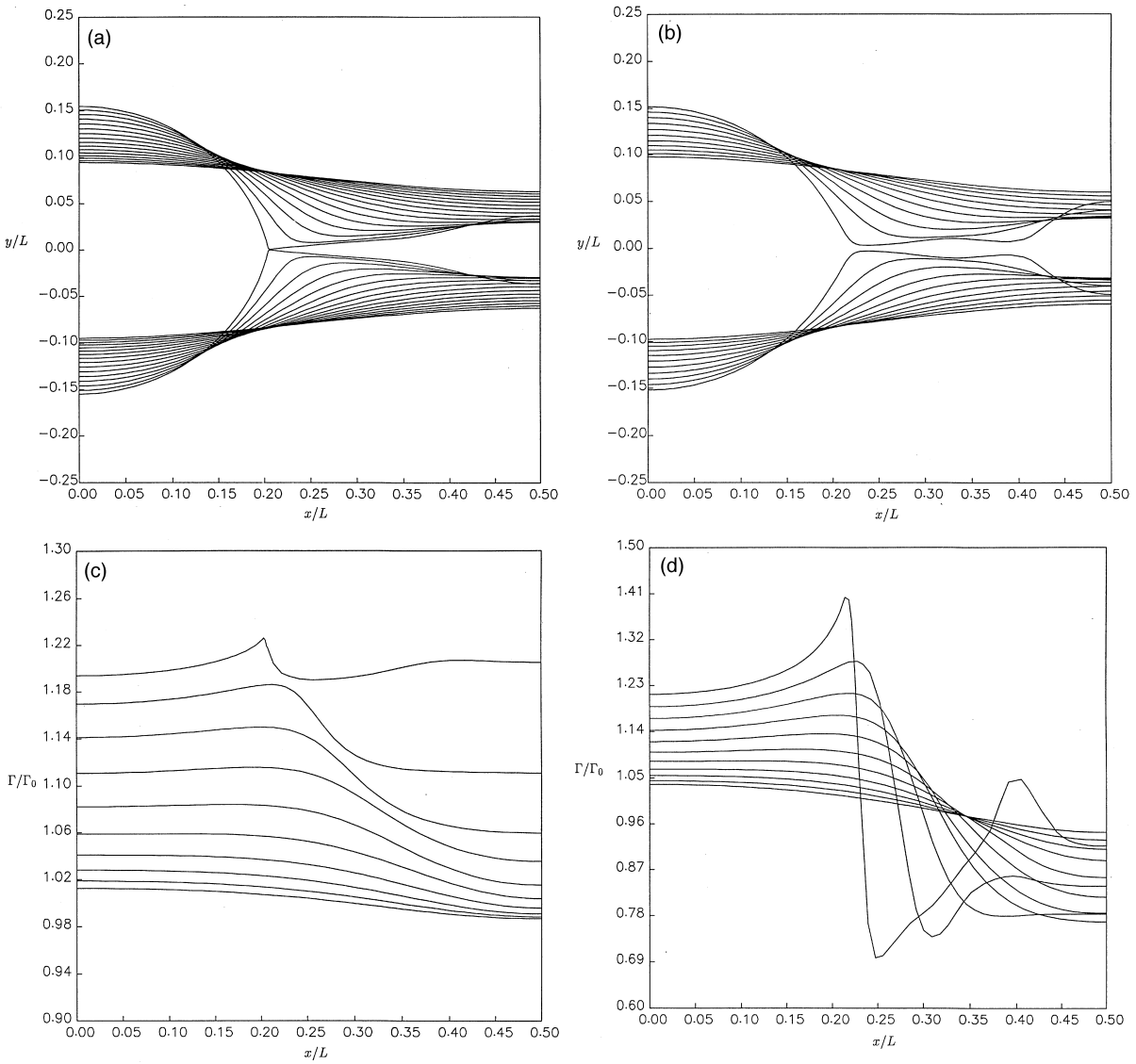

Fig. 7. Characteristic stages in the evolution of a thread and corresponding distribution of the surfactant for $\lambda = 1$, $\beta = 0.5$, subject to an unstable normal-mode disturbance with $ka = 0.5$ and $a_1/a = 0.2$; (a, c) $\alpha = 1$, and (b, d) $\alpha = 100$. L is the wavelength of the perturbation. The critical time for breakup is estimated to be $\hat{t}_c \cong 59.6$ for case (a) and $\hat{t}_c \cong 65.95$ for case (b).

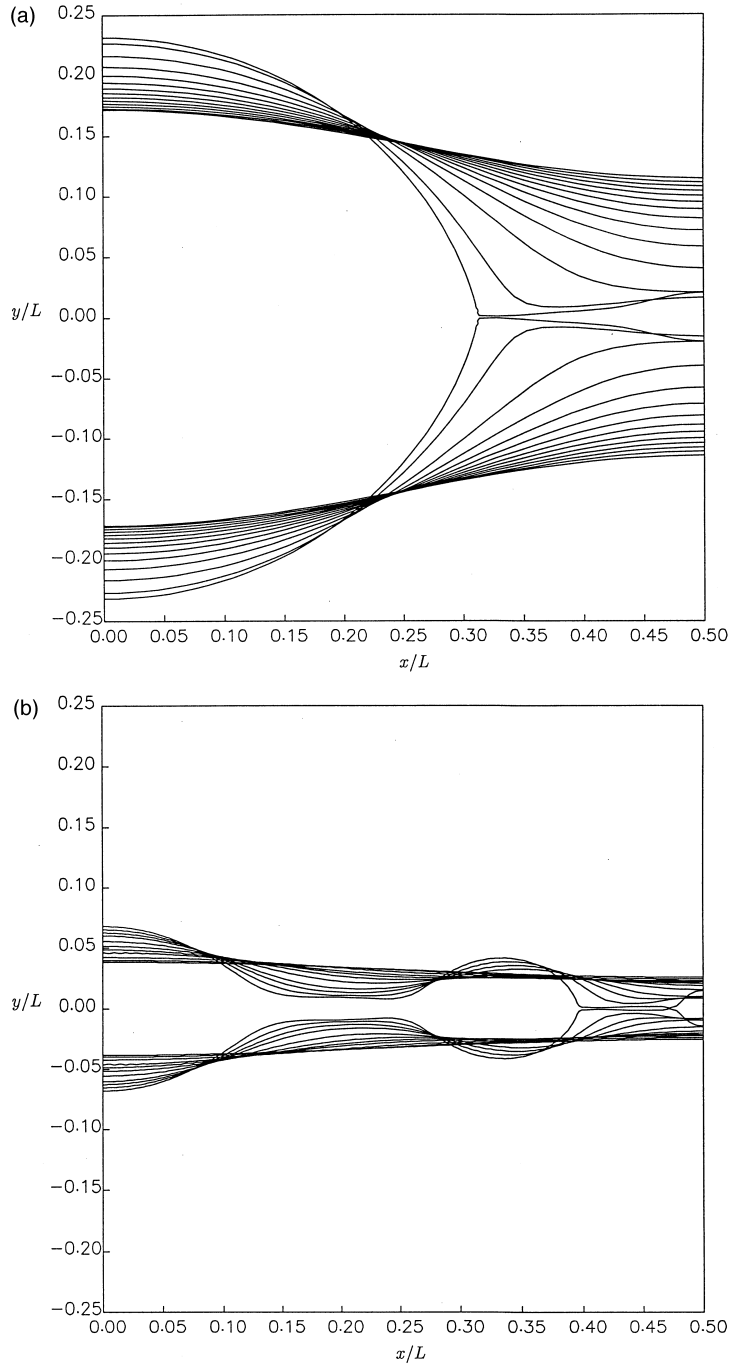

Fig. 8. Charactertic stages in the evolution of a thread for $\lambda = 1, \beta = 0.5, \alpha = 100$, and $a_1/a = 0.2$ subject to an unstable normal-mode disturbance with (a) $ka = 0.9$ and (b) $ka = 0.2$. The critical time for breakup is estimated to be $\hat{t}_c \cong 62.4$ for case (a) and $\hat{t}_c \cong 170$ for case (b).

not so small that subharmonic waves dominate, the thread breaks up in the middle of each period yielding one primary drop within each period, for a wide variety of conditions (Kwak, 1999). The motion for $\lambda = \infty$ will be discussed in the next section in the context of the instability of an annular layer.

The case $\lambda = 0$, corresponding to a viscous thread suspended in an inviscid ambient medium, deserves special attention. When the surface tension is constant, the instability causes the thread to keep thinning at the troughs of a sinusoidal perturbation, and then breakup at a finite time into a series of primary drops. Before breakup, the drops are connected by paraboloidal stems instead of spindle-like ligaments encountered earlier for $\lambda = 1$. A small amount of ambient-fluid viscosity causes the points of breakup to be shifted toward the base of the primary drops, as illustrated in Fig. 7(a) (e.g. Pozrikidis, 1999). In Fig. 9(a) and (b), we present typical stages in the evolution of a thread in the presence of a surfactant, for $\lambda = 0$, $\beta = 0.5$, $\alpha = 1, 100$, subject to a perturbation with $ka = 0.5$, and $a_1/a = 0.2$. The corresponding distributions of the surfactant concentration are shown in Fig. 9(c) and (d). When $\alpha = 1$, the motion is similar to that occurring under constant surface tension. When $\alpha = 100$, the nonuniformity of the surfactant distribution causes the primary drops to develop spindle-like shapes.

A graph of the amplitude ratio A/a_1 against the reduced time $\hat{t} = \gamma t/(a\mu)$ corresponding to the evolution illustrated in Fig. 9, reveals that the growth of the perturbation is nearly exponential almost up to the point of breakup, with the nonlinear motion being only slightly faster than that described by the linear theory (Kwak, 1999). In this case, nonlinear interactions promote the rate of interfacial deformation instead of leading to saturation. Similar behavior was observed for other values of viscosity ratio and parameters α and β.

Papageorgiou (1995) studied the evolution of a thread with constant surface tension γ suspended in an inviscid ambient fluid, corresponding to $\lambda = 0$, and discovered a similarity solution of a simplified system of differential equations that describes the asymptotic behavior near the critical time and around the critical location for breakup. The similarity solution predicts that the minimum radius of the thread decreases linearly in time according to the scaling law

$$f(x_c, t) \cong \frac{\gamma}{12(1+\beta_c)\mu}(t_c - t) \tag{46}$$

where x_c is the axial position where breakup is expected to occur, and t_c is the critical time for breakup. The value of the constant β_c arises by solving the nonlinear eigenvalue problem, and Papageorgiou found that the least unstable flow corresponds to $\beta_c = 0.175$. Pozrikidis (1998b) confirmed that the similarity solution describes the late stage of breakup for a broad range of generally non-monochromatic perturbations, but only when the viscosity ratio is precisely equal to zero.

The derivation of Eq. (46) relies on the assumption that the shear stress vanishes along the evolving interface, which requires that the surfactant is distributed uniformly over a distance that is sufficiently larger than the instantaneous minimum thread diameter. Referring to Fig. 9(c) and (d), we see that this assumption is satisfied to a good approximation: large gradients of the surfactant concentration near the point of breakup are not established. Another assumption underlying the derivation of Eq. (46) is that the surface tension is

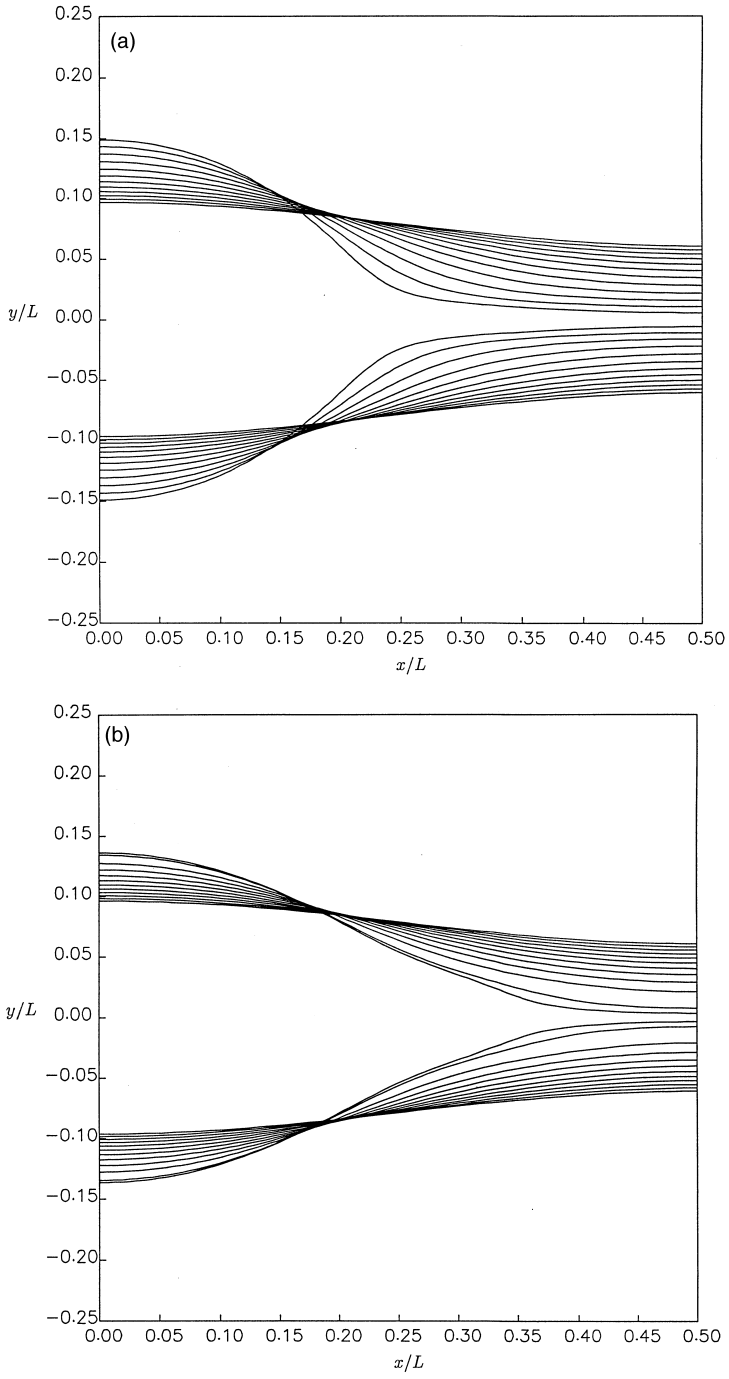

Fig. 9. Characteristic stages in the evolution of a thread and corresponding distribution of the surfactant for $\lambda = 0$, $\beta = 0.5$, subject to an unstable normal-mode perturbation with $ka = 0.5$ and $a_1/a = 0.2$; (a, c) $\alpha = 1$ and (b, d) $\alpha = 100$.

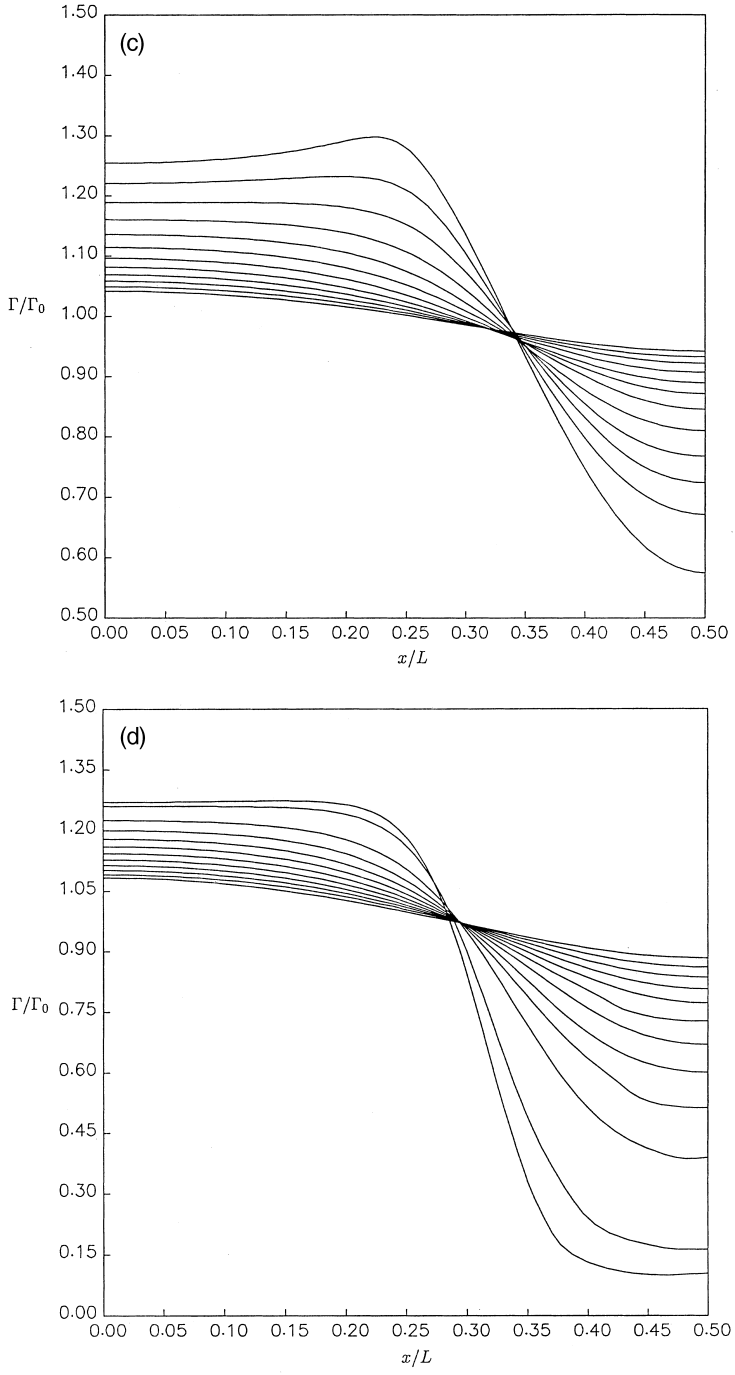

Fig. 9 (*continued*)

constant, or at least varies at a rate that is much less than the rate of thread thinning. In the present case, we expect that strong convection associated with the accelerating stagnation-point flow near the point of breakup will cause depletion of the surfactant from that region. It appears then reasonable to approximate the local surface tension with that corresponding to a clean interface. With this approximation, the scaling law (46) becomes

$$f(x_c t) \cong \frac{\gamma_0}{12(1-\beta)(1+\beta_c)\mu}(t_c - t) \tag{47}$$

In Fig. 10, we plot the reduced minimum radius of the thread occurring at the troughs of the imposed sinusoidal perturbation, and obtain strong numerical evidence that the thread will break up at a finite time. The dashed lines represent the predictions of the scaling law (46), with γ being the instantaneous value of the surface tension at the point of breakup at the end of the simulation, and the dotted lines represent the predictions of the scaling law (47). The agreement is good for $\alpha = 100$ corresponding to Fig. 10(b) where the dashed and dotted lines nearly coincide, but significant discrepancies are observed for $\alpha = 1$ corresponding to Fig. 10(a). It is possible that the solid line will asymptote to the dotted line in Fig. 10(a) at later times but, unfortunately, numerical difficulties did not allow us to continue the simulation and thus confirm this conjecture.

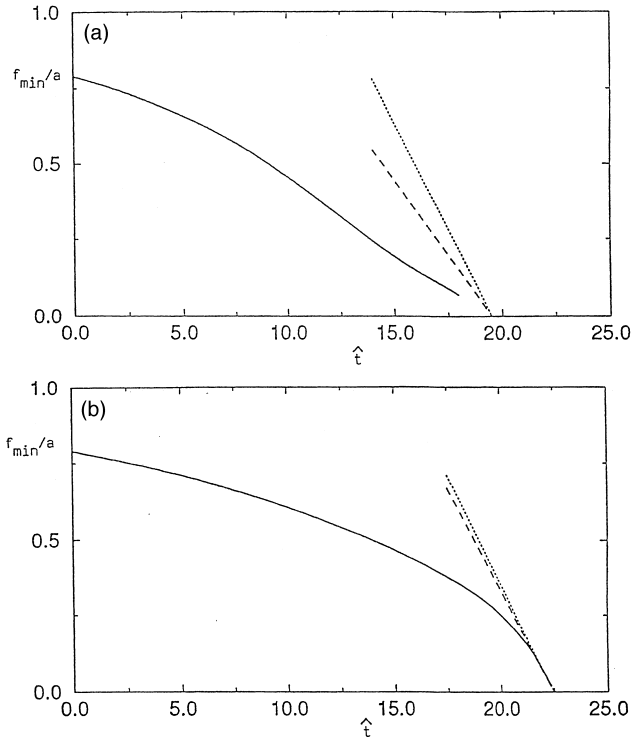

Fig. 10. Evolution of the minimum thread radius corresponding to Fig. 9; (a) $\alpha = 1$ and (b) $\alpha = 100$. The dotted and dashed lines represent, respectively, predictions of a similarity solution developed by Papageorgiou.

5. Instability of a film lining the interior surface of a cylindrical tube

In Section 2, we saw that the presence of a surfactant significantly reduces the growth rate of disturbances along the interface of an annular layer coated on the interior surface of a cylindrical tube. In this section, we consider the nonlinear growth of disturbances and study the effect of a surfactant on the long-time behavior of the core-annular arrangement. First, we use the boundary-integral method to simulate the evolution of the interface for viscosity ratio $\lambda = 1$. Second, we study the instability of a thin annular layer using an asymptotic flow model developed by Dumbleton and Hermans (1970), Carroll and Lucassen (1974) and Otis et al. (1990), applicable for long wave length perturbations. In both cases, we compare the numerical results with those obtained earlier for the unbounded thread and thereby assess the significance of the cylindrical boundary.

5.1. Boundary-integral simulations

The numerical method for simulating the motion of the interface in Stokes flow is similar to that outlined in Section 4. The main difference is that the kernel of the single-layer Stokes potential involves the periodic Green's function for Stokes flow inside a circular tube, which is available in the form of a rapidly converging series. Considerations of computational cost associated with the expensive evaluation of the Green's function required that we only consider cases where the viscosity of the annular fluid is equal to the viscosity of the core fluid.

It is well known that an annular layer may develop in two complementary ways. When the thickness of the layer is sufficiently small, the instability causes the development of a series of annular collars attached to the cylinder. When the thickness of the layer is sufficiently larger, the layer collapses into axisymmetric bridges extending across the tube, with collars possibly forming between adjacent bridges at longer times.

In Fig. 11(a) and (b), we present typical stages in the evolution of the interface of an annular layer with radius $a_e/a = 1.25$, subject to a normal-mode perturbation of initial amplitude $a_1/a = 0.1$ and wave number $ka = 0.7$, which is close to the wave number with the maximum linear growth rate. Because of the smallness of the magnitude of the growth rate and restrictions on the time step for numerical stability, each one of these simulations consumes several days of CPU time. For the simulation shown in Fig. 11(a), the interface is devoid of surfactants, whereas for the simulation shown in Fig. 11(b) surfactant is present with $\beta = 0.5$ and $\alpha = 100$. The annular layer is thick enough for the instability to lead to collapse in both cases. Fig. 11(a) and (b) shows that the presence of the surfactant does not have an important effect on the qualitative features of the evolution of the interface. Inspection of the times corresponding to the depicted profiles, however, shows that the presence of the surfactant considerably delays the growth of the interfacial waves, in agreement with the results of linear stability theory.

In Section 4, we saw that the wave number plays an important role in determining the number of drops developing after the breakup of an infinite thread. In the case of an annular layer, we find that the wave number plays a secondary role, irrespective of the presence of a surfactant: Long waves cause the interface to collapse at a single point over each period. Because of its reduced thickness, the thinned layer extending between two adjacent bridges is

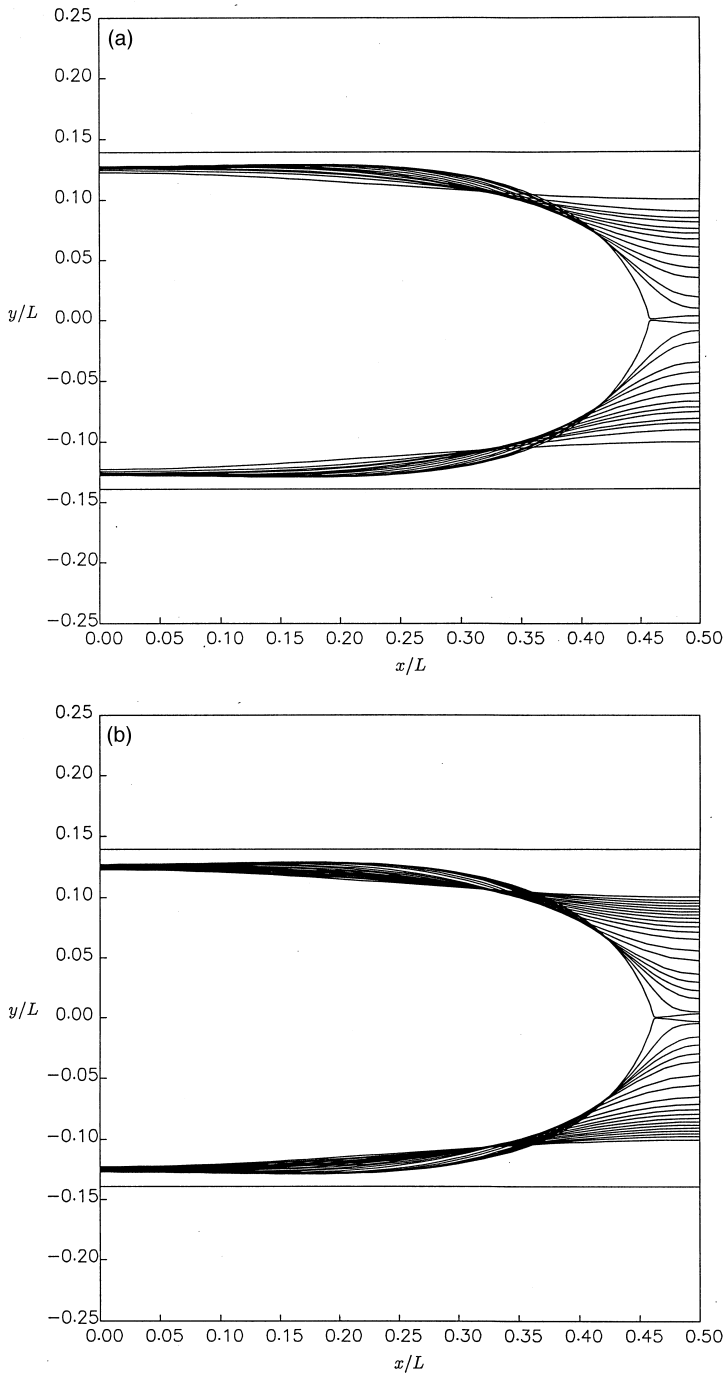

Fig. 11. Characteristic stages in the evolution of a core-annular arrangement for $a_e/a = 1.25$, (a) clean interface with $\lambda = 1$, $ka = 0.7$, and $a_1/a = 0.1$. The critical time for breakup is estimated to be $\hat{t}_c \cong 1861.25$; (b) surfactant contaminated interface with $\lambda = 1$, $\beta = 0.5$, $\alpha = 100$, $ka = 0.7$, and $a_1/a = 0.1$. The critical time for breakup is estimated to be $\hat{t}_c \cong 3965$.

expected to develop annular collars at long times. The developing distribution of the surfactant concentration is qualitatively similar to the case with shorter wave length like Fig. 11(b). The effect of the wave length and the presence of the surfactant become important when the thickness of the annular layer is comparable to the radius of the core. For example, when $a_e/a = 2.5$ the qualitative features of the motion are similar to those discussed in the preceding section for the unbounded thread (Kwak 1999).

5.2. Thin-layer approximation

When the thickness of an annular layer is sufficiently smaller than the axial length scale of an interfacial wave, the motion may be described under the approximation of locally unidirectional flow independent of the viscosity of the core fluid, as long as the viscosity of the annular layer is nonzero. Dumbleton and Hermans (1970) and Johnson et al. (1991) developed a system of equations governing the motion of the interface for constant surface tension; the second set of authors accounted for fluid inertia through an integral momentum balance. Carroll and Lucassen (1974) and Otis et al. (1990) extended this system to account for variable surface tension due to an insoluble surfactant. Otis et al. (1993) took into consideration the finite tube length and the time-dependence of the tube diameter.

In the presence of a surfactant, the lubrication model consists of the mass-conservation equation

$$\frac{\partial f}{\partial t} = \frac{\partial Q}{\partial x} \tag{48}$$

where $\sigma = f(x, t)$ describes the location of the interface and $\partial f/\partial x$ is sufficiently smaller than unity, complemented by the following expression for the flow rate:

$$Q = -\frac{\partial p_2}{\partial x}\frac{h^3}{2\mu_2}\left(\frac{2}{3} + \frac{\partial\gamma/\partial x}{h(-\partial p_2/\partial x)}\right) \tag{49}$$

where $h = a_e - f(x, t)$ is the local and instantaneous liquid layer thickness. The surface tension is related to the surfactant concentration by means of the constitutive equation (29), and the surfactant concentration evolves according to the equation

$$\frac{\partial \Gamma}{\partial t} = -\left(\frac{\partial(\Gamma u_x)}{\partial x}\right)_{\sigma=f} + D_s\frac{\partial^2 \Gamma}{\partial x^2} \tag{50}$$

where

$$u_x = -\frac{\partial p_2}{\partial x}\frac{h^2}{2\mu_2}\xi\left(2 + \frac{2\,\partial\gamma/\partial x}{h(-\partial p_2/\partial x)} - \xi\right) \tag{51}$$

is the axial velocity, and $\xi \equiv (a_e - \sigma)/h$ is the non-dimensional radial position measured from the tube up to the interface.

A normal mode linear stability analysis of the preceding set of equations, using the notation of Section 2, yields the following quadratic equation for the growth rate

$$(-ick)^2+\left[k^2D_s-A+\frac{\beta}{1-\beta}\gamma_0 B\right](-ick)-k^2D_sA+\frac{\beta}{1-\beta}\gamma_0 C=0 \tag{52}$$

where the coefficients A, B, and C are defined as

$$A=\frac{\gamma_{-1}}{3\mu_2}\frac{k^2h_0^3}{a^2}(1-k^2a^2),\quad B=\frac{k^2h_0}{\mu_2}\left(\frac{h_0}{2a}-1\right),\quad C=\frac{7}{12}\frac{\gamma_{-1}}{\mu_2}\frac{k^4h_0^4}{a^2}(1-k^2a^2) \tag{53}$$

The ratio of the amplitude of the perturbation in surface tension to the amplitude of the interface is given by

$$\frac{\gamma_1}{a_1}=\frac{\dfrac{k^2h_0^2}{2\mu_2}\dfrac{\gamma_0}{a^2}(1-k^2a^2)}{\dfrac{(1-\beta)\left[(-ick)+k^2D_s\right]}{\beta\gamma_0}+\dfrac{k^2h_0^2}{2a\mu_2}-\dfrac{k^2h_0}{\mu_2}} \tag{54}$$

Solving Eq. (52) provides us with two growth rates corresponding to a stable and a conditionally unstable normal mode. In the absence of a surfactant, we obtain a single growth rate that agrees with that derived by Dumbleton and Hermans (1970) and Johnson et al. (1991) for constant surface tension. The lubrication model is physically consistent, in the sense that the second mode is unstable for reduced wave numbers that are less than unity.

We carried out extensive comparisons between the growth rates predicted by Eq. (52) and those computed by solving the unsimplified eigenvalue problem for Stokes flow discussed in Section 2. When the viscosity of the core fluid is negligible, corresponding to viscosity ratio $\lambda=\infty$, and the radius of the unperturbed interface is 95% of the tube radius, the maximum difference in the growth rates over the entire range of unstable wave number $0<ka<1$ is on the order of 0.0001% in the presence or absence of a surfactant. When the radius of the interface is reduced to 90% of the tube radius, the maximum difference in the order of 0.001%. Johnson et al. (1991) observed similar agreement for the case of constant surface tension. When the radius of the interface is reduced to 50% of the tube radius, the long-wave model underestimates the growth rate by a factor of 0.5. Kwak (1999) tabulates the range of wave numbers where the two predictions agree up to a specified accuracy. In the limit of small wave numbers and small layer thicknesses, the asymptotic results based on the thin-layer model reduce to the exact results for any value of the viscosity ratio. For example, when $\lambda=1$ and $ka=0.1$, the growth rate predicted by the thin-layer model is 10% less than that arising from the unsimplified linear stability theory.

Otis et al. (1990) presented numerical solutions of the thin-layer equations computed by the semi-implicit Adams–Bashforth method. To directly compare the predictions of the thin-layer model with results of boundary integral simulations, we implemented a fully-implicit finite-difference method. The method is first-order accurate in time and second-order accurate in space, and incorporates adaptive node regridding that uses cubic-spline interpolation to resolve the fine features of the interface. Carrying out each time step requires solving a nonlinear system of algebraic equations which was done using Newton's method with the Jacobian evaluated by numerical differentiation. Further details on the numerical method are given by Kwak (1999).

In Fig. 12(a), we present stages in the instability of an annular layer in the absence of a surfactant computed subject to the thin-layer approximation, for $a_e/a = 1.25$, and for a perturbation with reduced wave number $ka = 0.7$ and amplitude $a_1/a = 0.10$. The evolving shape of the interface in the presence of a surfactant with $\beta = 0.5$ and $\alpha = 100$ is virtually identical. The results show that the annular layer collapses at a single point within each period yielding a liquid bridge. Inspection of Fig. 12(b), illustrating the evolution of the minimum radial position of the interface, however, shows once again that the presence of a surfactant considerably delays the growth of the interfacial waves, in agreement with the results of Otis et al. (1993). In the small pulmonary airways, the tube radius a_e corresponding to the total lung capacity is on the order of 0.025 cm, and α is on the order of 10^7. At this high value of α, surfactant diffusion is negligible compared to convection. Further simulations showed that the wave number plays a secondary role in determining the nature of the breakup (Kwak, 1999), as was observed for the case of $\lambda = 1$ discussed in the preceding subsection.

Comparing the profile shown in Fig. 12(a), corresponding to $\lambda = \infty$, with that shown in Fig. 11(a), corresponding to $\lambda = 1$, we observe significant differences during the later stages of collapse regarding, in particular, the location of the point of pinch-off. Previous work has established that, in the absence of a surfactant and under conditions of Stokes flow, a liquid column suspended in vacuum, corresponding to $\lambda = 0$, pinches off symmetrically. When $\lambda = 1$, the column pinches off unsymmetrically forming two conical structures on either side of the point of breakup, as shown in Fig. 11(a) (Newhouse and Pozrikidis 1992, Lister and Stone, 1998, Pozrikidis 1999). The simulations presented in Fig. 12(a) suggest that an inviscid column suspended in a viscous fluid, corresponding to $\lambda = \infty$, pinches off at a single point over each period. Boundary integral simulations for very high values of λ confirmed that this is also true for an unbounded thread in the absence or presence of surfactants and in the context of Stokes flow, as illustrated in Fig. 13. Now, in the two special cases $\lambda = 0$ or ∞ and in the absence of surfactant, maximum growth rate according to linear theory occurs at zero wave number, whereas for other values of λ maximum growth rate occurs at nonzero wave numbers. This observation suggests a tentative correspondence between the location of the wave number for maximum growth rate in the wave number space, and the geometrical symmetry of the interface on either side of the point of breakup.

6. Concluding remarks

The presence of a surfactant causes a discontinuity in the tangential component of the traction across an interface, and the induced motion tends to immobilize portions of the interface and to effectively raise the viscosity of the ambient fluid. The addition of a surfactant is known to reduce the deformation of a viscous drop in simple shear or extensional flow, in spite of the accumulation of the surfactant at the tips and the consequent reduction in local surface tension. In the case of a thread, the addition of a surfactant reduces the growth rate of the unstable mode, and the reduction is greatest when one of the fluids is inviscid. The numerical simulations presented in Section 5 suggest that, at $\lambda = 0$, the effect of the surfactant is not strong enough to alter the character of the motion during the late stages of the breakup relative to that observed for a clean interface where breakup occurs at the trough of the

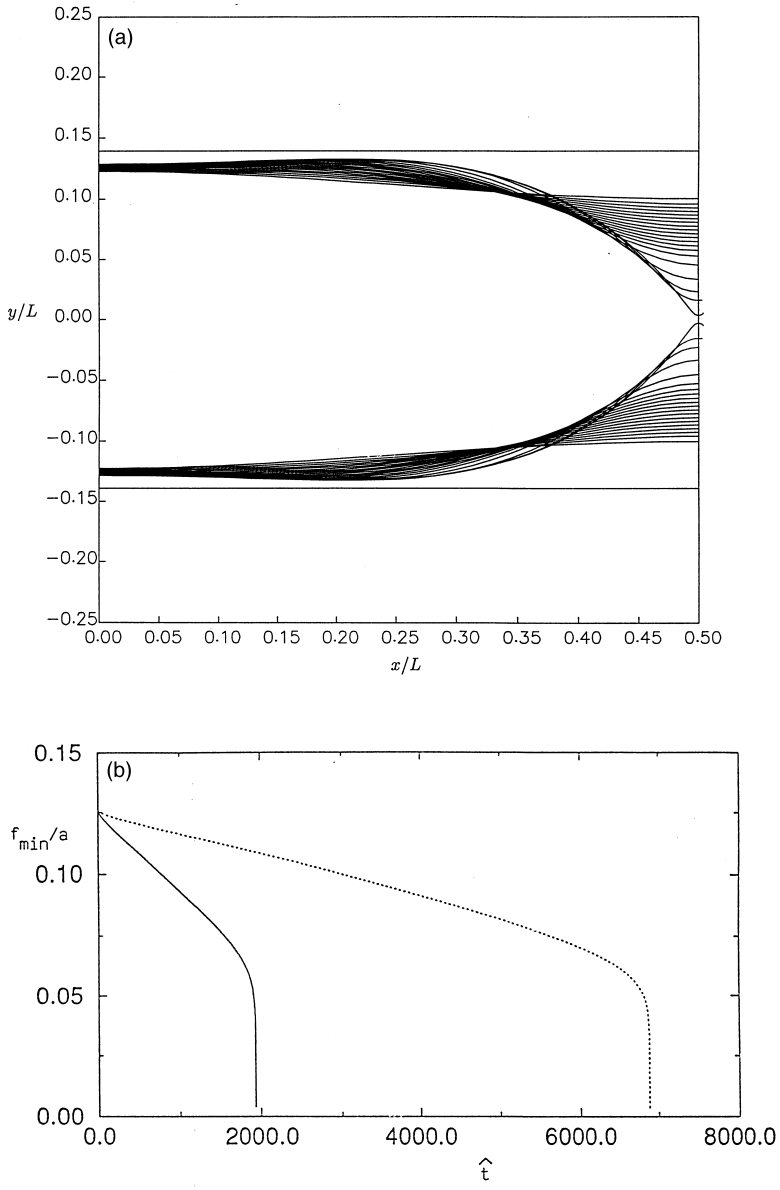

Fig. 12. Simulations based on the lubrication approximation for $a_e/a = 1.25$. (a) Characteristic stages in the evolution of the interface for $\lambda = \infty$, $\beta = 0$, $ka = 0.7$, and $a_1/a = 0.1$, at dimensionless times $\hat{t} = 0$, 125, 250,..., 1875.0, 1928.76, 1932.51, 1932.69, 1932.71. (b) Evolution of the minimum core radius corresponding to (a) drawn with the solid line; the dashed line shows the evolution for a contaminated interface with $\lambda = \infty$, $\beta = 0.5$, $\alpha = 100$, $ka = 0.7$, and $a_1/a = 0.1$.

sinusoidal perturbation. These results, however, were obtained with a linear relation between the surface tension and surfactant concentration; it is possible that a nonlinear relation will lead to a different type of behaviour.

Concerning the instability of an annular layer coated on the interior of a cylindrical tube with reference to the bronchial airways, we note that during breathing, the radius of the small airways changes from the maximum value corresponding to the total lung capacity to a smaller value. Since instability is initiated when the length of the airway becomes longer than $2\pi a$, where a is the instantaneous radius of the interface, the wave number is selected by the length of the airway and does not necessarily correspond to the most unstable normal mode. A comparison between the time scale of expiration t_{exp} and the time required for the annular layer to collapse t_{col} is appropriate only when the radius of the annular film and amplitude of the perturbation can be assessed with certainty. For the conditions corresponding to dotted line shown on Fig. 12(b), the time is on the order of $2 \times 10^3 \mu a/\gamma$. Using $\mu = 0.01$ dyn s/cm^2, $a = 0.025$ cm, and $\gamma = 30$ dyn/cm, we find $t_{\text{col}} = 0.017$ s which is much less than the period of normal breathing. Since, however, the time for collapse scales with the logarithm of the initial amplitude of the perturbation, a weaker disturbance would have caused collapse before inspiration. In the present as well as previous stability analyses, the amplitude of the perturbation was treated as an unspecified parameter and given an arbitrary value. This ambiguity can be eliminated by imposing the condition of temporal periodicity across each breathing cycle. This analysis of this periodic motion is under current investigation.

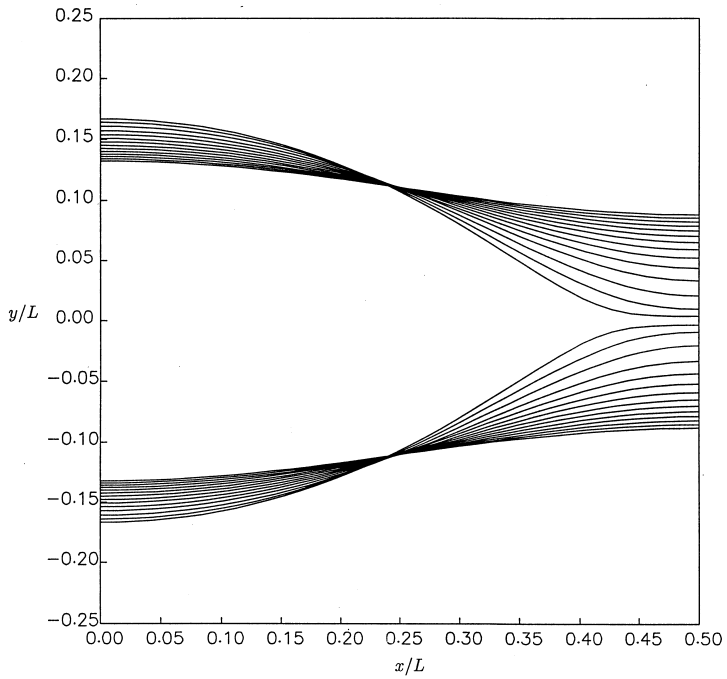

Fig. 13. Characteristic stages in the evolution of an infinite thread for $\lambda = 10{,}000$, $\beta = 0.5$, $\alpha = 10{,}000$, $ka = 0.7$ and $a_1/a = 0.2$. The final profile corresponds to $\hat{t} = 78{,}000$.

Acknowledgements

This research was supported by the National Science Foundation. Acknowledgment is made to the donors of the Petroleum Research Fund, administered by the American Chemical Society, for partial support.

Appendix A. Components of the secular matrix for Navier–Stokes flow

In this appendix, we present the expressions for the components of the matrix M defined in Eq. (34).

$$F_1 = -2\mu_1 k^2 I_1(ka) - \frac{\gamma_0 \beta k^2}{(1-\beta)\big(-ick + k^2 D_s\big)a}\big[kaI_0(ka) - I_1(ka)\big]$$

$$F_2 = -\mu_1\big(k^2 + k_1^2\big)I_1(k_1 a) - \frac{\gamma_0 \beta k^2}{(1-\beta)\big(-ick + k^2 D_s\big)a}\big[k_1 aI_0(k_1 a) - I_1(k_1 a)\big]$$

$$F_3 = -2\mu_1 k^2 K_1(ka) + \frac{\gamma_0 \beta k^2}{(1-\beta)\big(-ick + k^2 D_s\big)a}\big[kaK_0(ka) + K_1(ka)\big]$$

$$F_4 = -\mu_1\big(k^2 + k_1^2\big)K_1(k_1 a) + \frac{\gamma_0 \beta k^2}{(1-\beta)\big(-ikc + k^2 D_s\big)a}\big[k_1 aK_0(k_1 a) + K_1(k_1 a)\big]$$

$$F_5 = 2\mu_2 k^2 I_1(ka)$$

$$F_6 = \mu_2\big(k^2 + k_2^2\big)I_1(k_2 a)$$

$$F_7 = 2\mu_2 k^2 K_1(ka)$$

$$F_8 = \mu_2\big(k^2 + k_2^2\big)K_1(k_2 a)$$

$$G_1 = (-ikc)\rho_1 I_0(ka) + 2\mu_1 \frac{k}{a}\big[kaI_0(ka) - I_1(ka)\big]$$

$$-\frac{\gamma_0 k}{(-ikc)a^2}(1 - k^2 a^2)I_1(ka) - \frac{\gamma_0 \beta k}{(1-\beta)\big(-ikc + k^2 D_s\big)a^2}\big[kaI_0(ka) - I_1(ka)\big]$$

$$G_2 = 2\mu_1 \frac{k}{a}\big[k_1 aI_0(k_1 a) - I_1(k_1 a)\big]$$

$$-\frac{\gamma_0 k}{(-ikc)a^2}(1-k^2a^2)I_1(k_1a)-\frac{\gamma_0\beta k}{(1-\beta)\big(-ikc+k^2D_s\big)a^2}\big[k_1aI_0(k_1a)-I_1(k_1a)\big]$$

$$G_3=-(-ikc)\rho_1K_0(ka)-2\mu_1\frac{k}{a}\big[kaK_0(ka)+K_1(ka)\big]$$

$$-\frac{\gamma_0 k}{(-ikc)a^2}(1-k^2a^2)K_1(ka)+\frac{\gamma_0\beta k}{(1-\beta)\big(-ikc+k^2D_s\big)a^2}\big[kaK_0(ka)+K_1(ka)\big]$$

$$G_4=-2\mu_1\frac{k}{a}\big[k_1aK_0(k_1a)+K_1(k_1a)\big]$$

$$-\frac{\gamma_0 k}{(-ikc)a^2}(1-k^2a^2)K_1(k_1a)+\frac{\gamma_0\beta k}{(1-\beta)\big(-ikc+k^2D_s\big)a^2}\big[k_1aK_0(k_1a)+K_1(k_1a)\big]$$

$$G_5=-(-ikc)\rho_2I_0(ka)-2\mu_2\frac{k}{a}\big[kaI_0(ka)-I_1(ka)\big]$$

$$G_6=-2\mu_2\frac{k}{a}\big[k_2aI_0(k_2a)-I_1(k_2a)\big]$$

$$G_7=(-ikc)\rho_2K_0(ka)+2\mu_2\frac{k}{a}\big[k_2aK_0(k_2a)+K_1(k_2a)\big]$$

$$G_8=2\mu_2\frac{k}{a}\big[k_2aK_0(k_2a)+K_1(k_2a)\big]$$

Appendix B. Components of the secular matrices for Stokes flow

In this appendix, we present the expressions for the components of the matrices $\boldsymbol{M}$ defined in Eqs. (39) and (43).

$$H_1=\frac{1}{2}a\big[I_0(ka)+I_2(ka)\big]$$

$$H_2=-\frac{1}{2}a\big[K_0(ka)+K_2(ka)\big]$$

$$H_3=-\frac{1}{2}a\big[I_0(ka)+I_2(ka)\big]$$

$$H_4 = \frac{1}{2}a\big[K_0(ka) + K_2(ka)\big]$$

$$L_1 = I_0(ka) + kaI_1(ka) \qquad \hat{L}_1 = 2I_0(ka) + kaI_1(ka)$$

$$L_2 = -K_0(ka) + kaK_1(ka) \qquad \hat{L}_2 = 2K_0(ka) - kaK_1(ka)$$

$$L_3 = -I_0(ka) - kaI_1(ka) \qquad \hat{L}_3 = -2I_0(ka) - kaI_1(ka)$$

$$L_4 = K_0(ka) - kaK_1(ka) \qquad \hat{L}_4 = -2K_0(ka) + kaK_1(ka)$$

$$N_1 = \frac{1}{2}a_{\mathrm{i}}\big[I_0(ka_{\mathrm{i}}) + I_2(ka_{\mathrm{i}})\big]$$

$$N_2 = -\frac{1}{2}a_{\mathrm{i}}\big[K_0(ka_{\mathrm{i}}) + K_2(ka_{\mathrm{i}})\big]$$

$$N_3 = I_0(ka_{\mathrm{i}}) + ka_{\mathrm{i}}I_1(ka_{\mathrm{i}}) \qquad \hat{N}_3 = 2I_0(ka_{\mathrm{i}}) + ka_{\mathrm{i}}I_1(ka_{\mathrm{i}})$$

$$N_4 = -K_0(ka_{\mathrm{i}}) + ka_{\mathrm{i}}K_1(ka_{\mathrm{i}}) \qquad \hat{N}_4 = 2K_0(ka_{\mathrm{i}}) - ka_{\mathrm{i}}K_1(ka_{\mathrm{i}})$$

$$Q_1 = \frac{1}{2}a_{\mathrm{e}}\big[I_0(ka_{\mathrm{e}}) + I_2(ka_{\mathrm{e}})\big]$$

$$Q_2 = -\frac{1}{2}a_{\mathrm{e}}\big[K_0(ka_{\mathrm{e}}) + K_2(ka_{\mathrm{e}})\big]$$

$$Q_3 = I_0(ka_{\mathrm{e}}) + ka_{\mathrm{e}}I_1(ka_{\mathrm{e}}) \qquad \hat{Q}_3 = 2I_0(ka_{\mathrm{e}}) + ka_{\mathrm{e}}I_1(ka_{\mathrm{e}})$$

$$Q_4 = K_0(ka_{\mathrm{e}}) - ka_{\mathrm{e}}K_1(ka_{\mathrm{e}}) \qquad \hat{Q}_4 = 2K_0(ka_{\mathrm{e}}) - ka_{\mathrm{e}}K_1(ka_{\mathrm{e}})$$

$$S_1 = 2\mu_1 k^2 I_1(ka) + \frac{\gamma_0\beta k^2}{(1-\beta)\big(-ikc + k^2 D_{\mathrm{s}}\big)a}\big[kaI_0(ka) - I_1(ka)\big]$$

$$S_2 = 2\mu_1 k\, kaI_0(ka) + \frac{\gamma_0\beta k}{(1-\beta)\big(-ikc + k^2 D_{\mathrm{s}}\big)a}\big(1 + k^2a^2\big)I_1(ka)$$

$$\hat{S}_2 = \frac{1}{k}S_1 + S_2 = 2\mu_1 k\big[I_1(ka) + kaI_0(ka)\big] + \frac{\gamma_0\beta k}{(1-\beta)\big(-ikc + k^2 D_{\mathrm{s}}\big)a}ka\big[I_0(ka) + kaI_1(ka)\big]$$

$$S_3 = 2\mu_1 k^2 K_1(ka) - \frac{\gamma_0 \beta k^2}{(1-\beta)\big(-ikc + k^2 D_s\big)a}\big[kaK_0(ka) + K_1(ka)\big]$$

$$S_4 = -2\mu_1 k\, kaK_0(ka) + \frac{\gamma_0 \beta}{(1-\beta)\big(-ikc + k^2 D_s\big)a^2} ka\big(1 + k^2 a^2\big) K_1(ka)$$

$$\hat{S}_4 = -\frac{1}{k} S_3 - S_4 = 2\mu_1 k\big[kaK_0(ka) - K_1(ka)\big] + \frac{\gamma_0 \beta k^2}{(1-\beta)\big(-ikc + k^2 D_s\big)}\big[K_0(ka) - kaK_1(ka)\big]$$

$$S_5 = -2\mu_2 k^2 I_1(ka)$$

$$S_6 = -2\mu_2 k\, kaI_0(ka) \quad \hat{S}_6 = \frac{1}{k} S_5 + S_6 = -2\mu_2 k\big[I_1(ka) + kaI_0(ka)\big]$$

$$S_7 = -2\mu_2 k^2 K_1(ka)$$

$$S_8 = 2\mu_2 k\, kaK_0(ka) \quad \hat{S}_8 = -\frac{1}{k} S_7 - S_8 = -2\mu_2 k\big[kaK_0(ka) - k_1(ka)\big]$$

$$T_1 = 2\mu_1 \frac{k}{a}\big[kaI_0(ka) - I_1(ka)\big] - \frac{\gamma_0 k}{(-ick)a^2}(1 - k^2 a^2) I_1(ka)$$
$$- \frac{\gamma_0 \beta k}{(1-\beta)\big(-ikc + k^2 D_s\big)a^2}\big[kaI_0(ka) - I_1(ka)\big]$$

$$T_2 = 2\mu_1 \frac{1}{a}\big[-kaI_0(ka) + \big(1 + k^2 a^2\big) I_1(ka)\big] - \frac{\gamma_0}{(-ikc)a^2}(1 - k^2 a^2)\big[kaI_0(ka) - I_1(ka)\big]$$
$$- \frac{\gamma_0 \beta}{(1-\beta)\big(-ikc + k^2 D_s\big)a^2}\big(1 + k^2 a^2\big) I_1(ka)$$

$$\hat{T}_2 = \frac{1}{k} T_1 + T_2 = 2\mu_1 k\, kaI_1(ka) - \frac{\gamma_0 k}{(-ikc)a}(1 - k^2 a^2) I_0(ka)$$
$$- \frac{\gamma_0 \beta k}{(1-\beta)\big(-ikc + k^2 D_s\big)a}\big[I_0(ka) + kaI_1(ka)\big]$$

$$T_3 = -2\mu_1 \frac{k}{a}\big[kaK_0(ka) + K_1(ka)\big] - \frac{\gamma_0}{(-ikc)a^3} ka(1 - k^2 a^2) K_1(ka)$$
$$+ \frac{\gamma_0 \beta}{(1-\beta)\big(-ikc + k^2 D_s\big)a^3} ka\big[kaK_0(ka) + K_1(ka)\big]$$

$$T_4 = 2\mu_1 \frac{1}{a}\big[kaK_0(ka) + \big(1 + k^2a^2\big)K_1(ka)\big] + \frac{\gamma_0}{(-ikc)a^2}(1 - k^2a^2)\big[kaK_0(ka) + K_1(ka)\big]$$

$$- \frac{\gamma_0\beta}{(1-\beta)\big(-ikc + k^2D_s\big)a^2}\big(1 + k^2a^2\big)K_1(ka)$$

$$\hat{T}_4 = -\frac{1}{k}T_3 - T_4 = -2\mu_1 k\, kaK_1(ka) - \frac{\gamma_0 k}{(-ikc)a}(1 - k^2a^2)K_0(ka)$$

$$- \frac{\gamma_0\beta}{(1-\beta)\big(-ikc + k^2D_s\big)a^2}ka\big[K_0(ka) - kaK_1(ka)\big]$$

$$T_5 = -2\frac{\mu^2}{a^2}ka\big[kaI_0(ka) - I_1(ka)\big]$$

$$T_6 = -2\mu_2\frac{1}{a}\big[-kaI_0(ka) + \big(1 + k^2a^2\big)I_1(ka)\big] \quad \hat{T}_6 = \frac{1}{k}T_5 + T_6 = -2\mu_2 k\, kaI_1(ka)$$

$$T_7 = 2\frac{\mu^2}{a^2}ka\big[kaK_0(ka) + K_1(ka)\big]$$

$$T_8 = -2\mu_2\frac{1}{a}\big[kaK_0(ka) + \big(1 + k^2a^2\big)K_1(ka)\big] \quad \hat{T}_8 = 2\mu_2 k\, kaK_1(ka)$$

References

Adamson, A.W., 1982. Physical Chemistry of Surfaces. Wiley, New York.

Anshus, B.E., 1973. The effect of surfactants on the breakup of cylinders and jets. J. Colloid Interface Science 43, 113–121.

Burckholder, H.C., Berg, J.C., 1974. Effect of mass transfer on laminar jet breakup. Part I: Liquid jets is gases. Part II: Liquid jets in liquids. AIChE Journal 20, 863–880.

Carroll, B., Lucassen, J., 1974. Effect of surface dynamics on the process of droplet formation from supported and free liquid cylinders. J. Chem. Soc. Faraday Trans. 70, 1228–1239.

Coyle, R.W., Berg, J.C., Niwa, J.C., 1981. Liquid–Liquid breakup under conditions of relative motion, mass transfer and solute adsorption. Chem. Eng. Sci. 36, 19–28.

Dumbleton, J.A., Hermans, J.J., 1970. Capillary instability of a thin annular layer of liquid around a solid cylinder. Ind. Eng. Chem. Fund. 9, 466.

Eggers, J., 1997. Nonlinear dynamics and breakup of free-surface flows. Rev. Modern Phys. 69, 865–930.

Elemans, P.H.M., Janssen, J.M.H., Meijer, H.E.H., 1990. The measurement of interfacial tension in polymer/polymer systems: the breaking thread method. J. Rheol. 34, 1311–1325.

Goren, S.L., 1962. The instability of an annular layer thread of fluid. J. Fluid Mech. 12, 309–319.

Grotberg, J.B., 1994. Pulmonary flow and transport phenomena. Annu. Rev. Fluid Mech. 26, 529–571.

Hajiloo, A., Ramamohan, T.R., Slattery, J.C., 1987. Effect of interfacial viscosities on the stability of a liquid thread. J. Colloid. Interface Science 117, 384–393.

Halpern, D., Grotberg, J.B., 1993. Surfactant effects on fluid-elastic instabilities of liquid-lined flexible tubes: a model of airway closure. J. Biomed. Eng. 115, 271–277.
Hansen, S., Peters, G.W.M, Meijer, H.E.H., 1999. The effect of surfactant on the stability of a fluid filament embedded in a viscous fluid. J. Fluid Mech. 382, 331–349.
Hlastala, M.P., Berger, A.J., 1996. Physiology of Respiration. Oxford University Press, London.
Janssen, J.J., Boon, A., Agterof, G.M., 1999. Influence of dynamic interfacial properties on droplet breakup in simple shear flow. AIChE. J. 40, 1929–1939.
Johnson, M., Kamm, R.D., Ho, L.W., Shapiro, A., Pedley, T.J., 1991. The nonlinear growth of surface-tension-driven instabilities of a thin annular layer. J. Fluid Mech. 223, 141–156.
Kwak, S., 1999. Studies of Viscous Interfacial Flow. Doctoral Dissertation, University of California, San Diego.
Lin, S.P., Reitz, R.D., 1998. Drop and spray formation from a liquid jet. Ann. Rev. Fluid Mech. 30, 85–105.
Lister, J.R., Stone, H.A., 1998. Capillary breakup of a viscous thread surrounded by another viscous fluid. Phys. Fluids 10, 2758–2764.
Milliken, W.J., Stone, H.A., Leal, L.G., 1993. The effect of surfactant on the transient motion of Newtonian drops. Phys. Fluids A 5, 69–79.
Nelson, N.K., Berg, J.C., 1982. The effect of chemical reaction on the breakup of liquid jets. Chem. Eng. Sci. 37, 1067–1078.
Newhouse, L.A., Pozrikidis, C., 1992. The capillary instability of annular layers and liquid threads. J. Fluid Mech. 242, 193–209.
Otis Jr., D.R., Johnson, M., Pedley, T.J., Kamm, R.D., 1990. The effect of surfactant on liquid film stability in the peripheral airways. Adv. Bioeng. 17, 55–57.
Otis Jr., D.R., Johnson, M., Pedley, T.J., Kamm, R.D., 1993. Role of pulmonary surfactant in airway closure: a computational study. J. Appl. Physiology 75, 1323–1333.
Palierne, J.F., Lequeux, F., 1991. Sausage instability of a thread in a matrix; linear theory for viscoelastic fluids and interface. J. Non-Newton. Fluid Mech. 40, 289–306.
Papageorgiou, D.T., 1995. On the breakup of viscous liquid threads. Phys. Fluids 7, 1529–1544.
Papageorgiou, D.T., 1996. Description of jet breakup. In: Renardy, Y.Y., Coward, A.C., Papageorgiou, D.T., Sun, S.M. (Eds.), Adv. Multi-Fluid Flows. SIAM, Philadelphia.
Pozrikidis, C., 1998. Numerical studies of cusp formation at fluid interfaces in Stokes flow. J. Fluid Mech. 357, 29–57.
Pozrikidis, C., 1999. Capillary instability and breakup of a viscous thread. J. Eng. Math. 36, 255–275.
Quéré, D., 1999. Fluid coating on a fiber. Annu. Rev. Fluid Mech. 31, 347–384.
Rabinovich, L.M., 1979. Effect of soluble surface-active substances on the stability of liquid films and jets. Fluid Dynamics 15, 816–822.
Rayleigh, L., 1878. On the instability of jets. Proc. London Math. Soc. 10, 4–13.
Rayleigh, L., 1892. On the stability of a cylinder of viscous liquid under capillary force. Phil. Mag. 34, 145.
Skelland, A.H.P., Walker, P.G., 1989. The effects of surface active agents on jet breakup in liquid–liquid systems. Can. J. Chem. Eng. 67, 762–770.
Skelland, A.H.P., Slaymaker, E.A., 1990. Effects of surface-active agents on drop size in liquid–liquid systems. Ind. Eng. Chem. Res. 29, 494–499.
Tarr, L.E., Berg, J.C., 1980. The effect of nonlinear concentration profiles on the breakup of jets undergoing mass transfer. Chem. Eng. Sci. 35, 1465–1467.
Tomotika, S., 1935. On the instability of a cylindrical thread of a viscous liquid surrounded by another viscous fluid. Proc. Roy. Soc. A 150, 322–337.
Weber, Z.Z., 1931. Zum Zerfall eines Flfssigkeitsstrahles. Z. Math. Mech. 11, 136–154.
Yarin, A.L., 1993. Free Liquid Jets and Films: Hydrodynamics and Rheology. Longman, New York.
Yap, D.Y.K., Gaver III, D.P., 1998. The influence of surfactant on two-phase flow in a flexible-walled channel under bulk equilibrium conditions. Phys. Fluids 10, 1846–1863.
Walstra, P., 1993. Principles of emulsion formation. Chem. Eng. Sci. 48, 333–349.
Whitaker, S., 1976. Studies of drop-weight method for surfactant solutions. Part III. Drop stability, the effect of surfactants on the stability of a column of liquid. J. Colloid Interface Science 54, 231–248.